Doctoral Dissertation (Shinshu University)

Study on Improved Mechanical Properties of Electrospun Nanofiber Membranes

March, 2014

Interdisciplinary Graduate School of Science and Technology, Shinshu University

Department of Bioscience and Textile Technology

Naotaka Kimura

Contents

Chapter 1

Introduction

1.1 Introduction

So what exactly is nanotechnology? Most definitions revolve around the study and control of phenomena and materials at length scales and sizes below 100 nm as seen in Figure 1. If the 20th century was the age of micro-technology, such as computer, gene, and development of new materials, the 21th century is the age of nano-technology of controlling billionth meter that will develop a new generation. Nanotechnology that changed fundamentally the way of thinking of scientists, such as physical, chemical, biological, and technical, is excellent technology that developed atomic and molecular world. As a result, they tried to establish two strategies, the process of top-down and bottom-up, which were approaches in order to create molecular nano-materials with artificial specific properties. Therefore, it all comes down to fundamental technology of new science that aims the interaction control of between atoms. Nanotechnology products that are on the market today are mostly gradually improved many products where some form of nanotechnology enabled material or process is used in the manufacturing process. The most important requirement for the nanotechnology definition is that the nanostructure has specific properties that are exclusively due to its nano-scale or –size proportions. Nanotechnology is come off as nothing more than so far way to be one elemental part of human life. However, the fibers that have submicron scale in diameter, so-called nanofiber, can have been already developed to a wide range of applications, such as filter [1, 2], biomedical [3, 4], catalysts [5, 6], electronics [7, 8], renewable energy [9, 10], and tissue engineering [11, 12]. The rapid progress of fiber technology can be expected to conduct advancement of life quality from a standpoint of materials science.

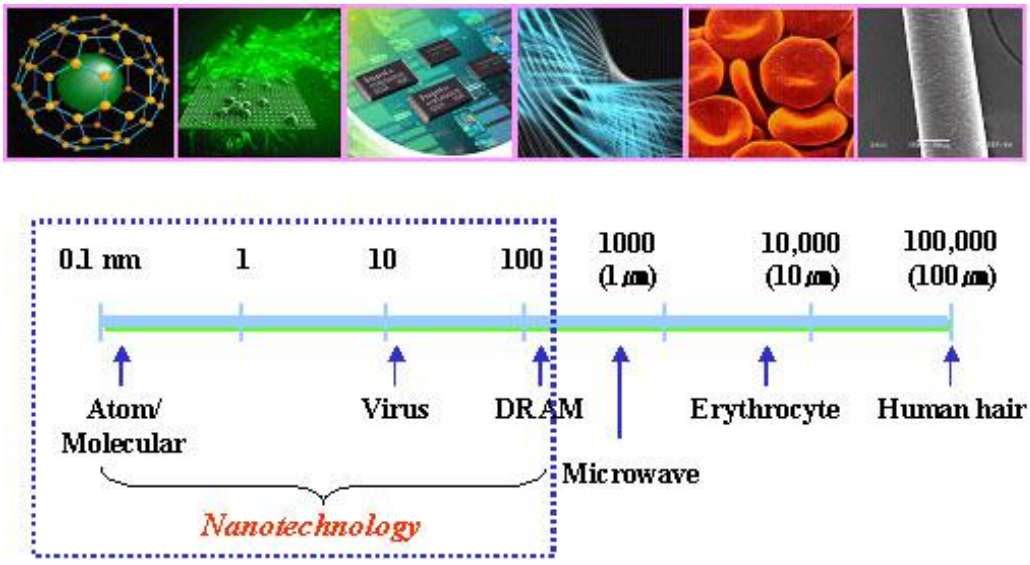

Figure 1 Nanotechnology definition.

There are many methods that produce nanofibers, such as Template synthesis [13, 14], Drawing [13, 15], Self-assembly [13, 16, 17], and Electrospinning [13, 18]. Template synthesis method can produce nano-tube and /or nano-fibril from various materials, such as conductive polymer, metal, semi-conductor, and carbon. Drawing method is similar to dry spinning on fiber industry, and can fabricate very long one nanofiber in incremental steps. However, this method has superiority only when viscous elasticity materials with adherence property that can endure load during pressuring and drawn process. Self-assembly method uses a molecular natural reaction by pattern, function, and macroscopic aggregation of materials. It is crucially important thing that need a long time in an effort to form continuous macromolecular nano-structure in this process. Finally, it is well-known as critically superiority because electrospinning method can fabricate mass production of nanofiber continuously from various polymer, inorganic, and hybrid materials. Electrospinning in one of fabrication technology of nanofiber has great attention as continuously and accomplishable technology of aimed all kinds of configuration. Since the electrospinning process was first patented in 1934 year by Formhals [19], it has been relatively neglected until 1970 year, and after which innovative research progress was not reported until early 1990s. The research group of Reneker from University of Akron reported that electrospinning process is capable for mass production of nanofibers. As a result, this method began to attract the attention of many researchers.

Electrospinning is a fabrication process of nanofibers through the electrically charged jet of polymer solution or melt. It is a unique approach of using electrostatic forces to produce fine fibers. The polymer fibers with sub-micron in diameters down to a few dozens of nanometers can be prepared by electrospinning. When the distribution of

fiber diameters is decreased from micrometers to nanometers, they show several amazing characteristics such as very huge surface area to volume ratio, flexibility inner surface functionalities, and superior mechanical performance [20]. The apparatus used for electrospinning is simply constructed (shown in Figure 2), which consists of a high voltage electric source with positive or negative polarity to provide a sufficient pulling force of the solution from the syringe or pipette to the spinneret, and finally to a conducting metal collector. The principle of nanofiber formation from polymer solution in this process in details is below. Polymer solution is forced to form a pendant drop of that one at the tip of the capillary. High voltage is applied to the polymer solution through an immersed electrode, thereby inducing free charges into the polymer solution. These charged ions move towards the electrode of opposite polarity in response to the applied electric field, and transferring pulling forces to the polymer liquid. At the tip of the capillary, the pendant polymer drop takes a cone in the presence of an electric field. This droplet was called Taylor cone. When the applied potential reaches a critical value that required for overcome the surface tension of the liquid, a jet of liquid is ejected from the tip of Taylor cone (shown in Figure 3). The production of nanofibers by the electrospinning process is influenced solution parameters (concentration, molecular weight, viscosity, surface tension, and conductivity), processing parameters (applied voltage, flow rate, types of collectors, and tip to collector distance), and ambient parameters (temperature and humidity). The collector can be made in any shape according to the requirements, such as rotating drum, flat plate, and parallel plate.

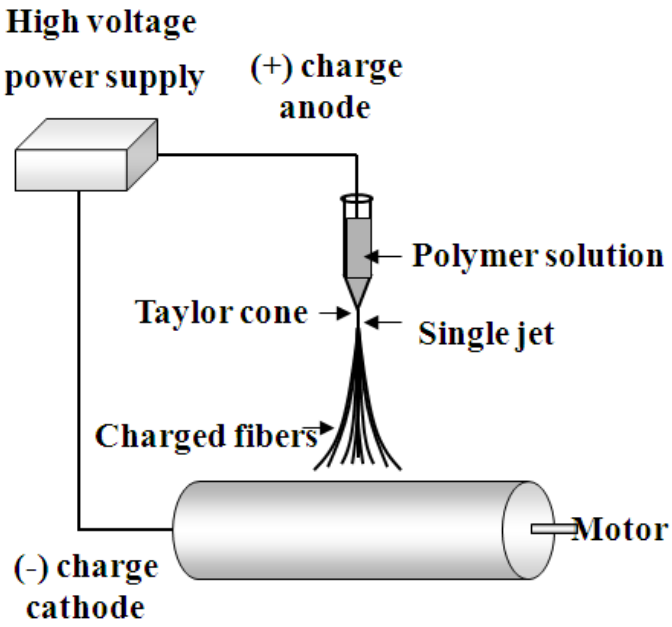

Figure 2 Schematic of electrospinning method.

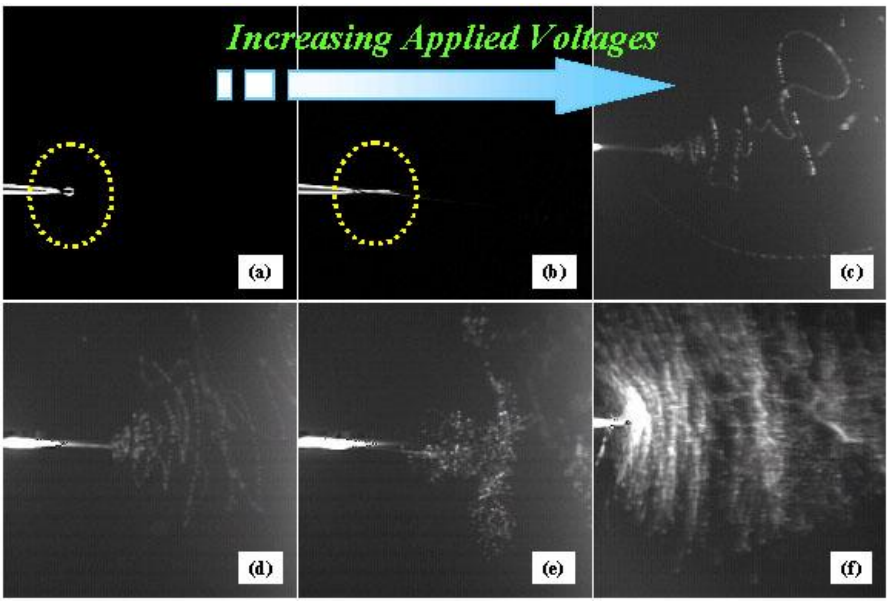

Figure 3 Phenomenon of fiber formation as a function of the applied voltages during electrospinning process; (a) 0, (b) 3, (c) and (d) 7, (e) 10, and (f) 15 kV, respectively.

Though electrospun nanofiber membrane have many great characteristic, such as high-specific surface area, high porosity, and hierarchical structure, it cannot be used only single to the practical application because its mechanical properties is exceptionally-low. The electrospun nanofibers are expected to apply a wide range of intended purpose. However, widespread adoption of these materials has been hindered by poor mechanical strength thus necessitating the use of an additional support layer which can add to membrane thickness and resistance. The poor mechanical strength of electrospun nanofibers are mostly due to their high porosity compounded with weak bonding at fiber junctions. Huang, et al. [21] reported a less invasive post-treatment approach to weld the fibers and demonstrated to enhance the strength of junction points without greatly changing the membrane morphology and dimension. This post-treatment involves the use of solvent vapor. It was concluded that solvent plays an important role in determining mechanical properties of electrospun PAN nanofiber membranes. By means of the method previously described, the tensile strength of electrospun PAN nanofiber membranes had over 20 MPa that could practically-use, and was greatly improved. Choi, et al. [22] reported application of electrospun PVDF nanofiber webs as an electrolyte binder or a separator for a battery. The electrospun PVDF nanofiber web was thermally treated at 160 ^{o}C for 2 h to improve the physical property and dimensional stability, and degree of crystallinity of the electrospun PVDF nanofiber was increased by the thermal treatment. This thermally treated electrospun PVDF nanofibers were higher around three times than untreated that one. Additionally, You, et al. [23] demonstrated that the PLLA nanofibers were thermally bonded at 180 °C and they were physically welded by thermal treatment without severe structural modification. As a result, the mechanical properties of thermally bonded membranes are a manifestation of the nature and quality of bonding

regions. PLLA nanofiber membrane treated at 180 °C for 15 min had higher the ultimate stress and the energy to rupture than untreated that one. As will be appreciated from the foregoing, the electrospun nanofibers are studied to improve the mechanical properties by various approaches because it is considered that there are a number of people would like to take advantage of the specific characteristics of them. Therefore, the focus of this study is “Improved mechanical properties of electrospun nanofiber membrane”.

1.2 References

[1] W. Sambaer, M. Zatloukal, D. Kimmer, 3D modeling of filtration process via polyurethane nanofiber based nonwoven filters prepared by electrospinning process, Chem Eng Sci. 66 (2011) 613-623.

[2] D. Aussawasathien, C. Teerawattananon, A. Vongachariy, Separation of micron to sub-micron particles from water: Electrospun nylon-6 nanofibrous membranes as pre-filters, J. Membr. Sci. 315 (2008) 11-19.

[3] R. Nirmala, R. Navamathavan, H.-S. Kang, M.H. El-Newehy, H.-Y. Kim, Preparation of polyamide-6/chitosan composite nanofibers by a single solvent system via electrospinning for biomedical applications, Coll. Surf. B 83 (2011) 173-178.

[4] S. Wang, X. Cao, M. Shen, R. Cuo, I. Banyai, X. Shi, Fabrication and morphology control of electrospun poly(γ-glutamic acid) nanofibers for biomedical applications, Coll. Surf. B 89 (2012) 254-264.

[5] X. Fnag, H. Ma, S. Xiao, M. Shen, R. Guo, X. Cao, X. Shi, Facile immobilization of gold nanoparticles into electrospun polyethyleneimine/polyvinyl alcohol nanofibers for catalytic applications, J. Mater. Chem. 21 (2011) 4493-4501.

[6] S. Chuangchote, J. Jitputti, R. Sagawa, S. Yoshikawa, Photocatalytic Activity for Hydrogen Evolution of Electrospun TiO_2 Nanofibers, Appl. Mater. Inter. 1 (2009) 1140-1143.

[7] H. Wu, L. Hu, M.W. Rowell, D. Kong, J.J. Cha, J.R. McDonough, J. Zhu, Y. Yang, M.D. McGehee, Y. Cui, Electrospun Metal Nanofiber Webs as

High-Performance Transparent Electrode, Nano Lett. 10 (2010) 4242-4248.

[8] M. Li, J. Zhang, H. Zhang, Y. Liu, C. Wang, X. Xu, Y. Tang, B. Yang, Electrospinning: A Facile Method to Disperse Fluorescent Quantum Dots in Nanofibers without Forster Resonance Energy Transfer, Adv. Funct. Mater. 17 (2007) 3650-3656.

[9] M. Inagaki, Y. Yang, F. Kang, Carbon Nanofibers Prepared via Electrospinning, Adv. Mater. 24 (2012) 2547-2566.

[10] M. Zhi, A. Manivannan, F. Meng, N. Wu, Highly conductive electrospun carbon nanofiber/MnO_2 coaxial nano-cables for high energy and power density supercapacitors, J. Power Sour. 208 (2012) 345-353.

[11] M.P. Prabhakaran, J.R. Venugopal, S. Ramakrishna, Mesenchymal stem cell differentiation to neuronal cells on electrospun nanofibrous substrates for nerve tissue engineering, biomater. 30 (2009) 4996-5003.

[12] J.-P. Chen, C.-H. Su, Surface modification of electrospun PLLA nanofibers by plasma treatment and cationized gelatin immobilization for cartilage tissue engineering, Acta Biomater. 7 (22011) 234-243.

[13] Z.-M. Hung, Y.-Z. Zhang, M. Kotaki, S. Ramakrishna, A review on polymer nanofibers by electrospinning and their applications in nanocomposites, Comp. Sci. Technol. 63 (2003) 2223-2253.

[14] A.A. Demkov, O.F. Sankey, Recent Developments in the Theory of Supralattices, Chem. Mater. 8 (1996) 1793-1806.

[15] T. Ondarcuhu, C. Joachim, Drawing a single nanofiber over hundreds of microns, Europhys. Lett. 42 (1998) 215-220.

[16] G.M. Whitesides, B. Grzybowski, Self-Assembly at All Scales, Science 295

(2002) 2418-2421.

[17] S. Zhang, Fabrication of novel biomaterials through molecular self-assembly, Nat. Biotechnol. 21 (2003) 1171-1178.

[18] P.K. Baumgarten, Electrostatic Spinning of Acylic Microfibers, J. Coll. Interf. Sci. 36 (1971) 71-79.

[19] A. Formhals, U.S. Patent 1975, 504; 1934.

[20] J.-H. He, Y.-Q. Wan, L. Xu, Nano-effects, quantum-like properties in electrospun nanofibers, Chaos, Solitions & Franctals 33 (2007) 26-37.

[21] L. Huang, S.S. Manickam, J.R. McCutcheon, Increasing strength of electrospun nanofiber membranes for water filtration using solvent vapor, J. Membr. Sci. 436 (2013) 213-220.

[22] S.S. Choi, Y.S. Lee, C.W. Joo, S.G. Lee, J.K. Park, K.S. Han, Electrospun PVDF nanofiber web as polymer electrolyte or separator, Electrochim. Acta 50 (2004) 339-343.

[23] Y. You, S.W. Lee, S.J. Lee, W.H. Park, Thermal interfiber bonding of electrospun poly (L-lactic acid) nanofibers, Mater. Lett. 60 (2006) 1331-1333.

1.3 Constitution of major study

Chapter 2: Molecular Orientation and Crystalline Structure of Aligned Electrospun Nylon-6 Nanofibers: Effect of Gap Size.

In this chapter, I investigated the effect of the gap size on the molecular orientation and crystalline structure of uniaxially well-aligned nylon-6 nanofibers produced in the gap between negatively charged metal plates. It followed that the size of this nylon-6 nanofiber membranes produced by using this collector too small to be practically and it has only limited in this study. However, well-aligned nylon-6 nanofiber membrane has been possessing molecular orientation in nylon-6 nanofiber. That is to say, this study was a significant because it is considered that aligned nanofiber membrane with the potentiality of improving mechanical properties.

Chapter 3: Improved the Mechanical properties of Isotactic poly (4-methyl-1-pentene) (PMP) fibrous Membrane Inducing Thermal-treatment and Stretching process.

In this chapter, electrospun isotactic poly (4-methyl-1-pentene) (PMP) fibrous membrane was fabricated, and then treated by heating and stretching process in order to make aligned fibrous membrane because well-aligned fibrous membrane had molecular orientation in each fiber as stated in chapter 2. Furthermore, it has been regarded as difficult to dissolve PMP, polyolefin, in organic solvent for using in electrospinning because of having high chemical resistance and electrical resistivity. Therefore, electrospun PMP fibrous membrane that improved mechanical properties has possibility

to be used a wide range of applications.

Chapter 4: Effects of Fe^{2+} ions on morphologies, microstructures and mechanical properties of electrospun nylon-6 nanofibers.

In this chapter, nylon-6 nanofiber mats containing Fe^{2+} ions were fabricated via electrospinning. Metal particles in nylon-6 nanofiber prevented from fiber fracture because it was considered that interrupted displacement of fracture. Additionally, the method in this study for improving the mechanical properties has a very simple in add-only metallic salt, and accomplished improvement of mechanical properties.

Chapter 5: Fabrication and characterization of reinforced electrospun poly (vinylidene fluoride-cohexafluoropropylene) nanofiber membranes

In this chapter, poly (vinylidene fluoride-co-hexafluoropropylene) (PVDF-HFP) nanofiber membranes with different amounts of polyethylene glycol (PEG) and polyethylene glycol dimethacrylate (PEGDMA) oligomer were fabricated via electrospinning. Recently, electrospun nanofiber has been studied for using battery separator. However, only making electrospun nanofiber membrane normally, it cannot be practically. Therefore, electrospun PVDF-HFP nanofiber membrane was improved by producing physically bonded structures and chemically cross-linked networks.

Chapter 2

Molecular Orientation and Crystalline Structure of Aligned Electrospun Nylon-6 Nanofibers: Effect of Gap Size.

Chapter 2

Molecular Orientation and Crystalline Structure of Aligned Electrospun Nylon-6 Nanofibers: Effect of Gap Size.

ABSTRACT

We study the effect of the gap size on the molecular orientation and crystalline structure of uniaxially well-aligned nylon-6 nanofibers produced in the gap between negatively charged metal plates. The relative intensities of several absorbance bands are found to be different in the parallel- and perpendicularly polarized FTIR spectra. X-ray analysis indicates that the metastable γ-form is predominant in as-spun nylon-6 nanofibers, and is transformed into the thermodynamically stable α-form by increasing the gap size. The polymer chains are thought to be oriented perpendicular to the fiber direction, and the molecular orientation to the fiber axis is enhanced on increasing the gap size.

2.1 Introduction

Nylon-6, as an engineering plastic, is one of three major, synthetic polymers in the fiber industry, and is also widely used in film manufacturing [1]. As shown in Figure 1, the molecular structure of nylon-6 consists of amide groups (CO-NH) separated by linear chains of methylene units [-$(CH_2)_5$-], and all of the amide groups are oriented approximately perpendicular to the polymer-chain axis. These groups provide the intermolecular hydrogen bonding between neighboring polymer chains, giving nylon some of its unique properties. Nylon-6 is therefore very similar in structure to the β-sheet conformation of natural polypeptides. Also, it is well known that nylon-6 exhibits crystalline structures of two different types: the a- and γ-forms. It has been reported that the α-form exhibits two characteristic reflections in Wide Angle X-ray diffraction (WAXD) at 2θ=20.2 and 23.0^o, whereas the g-form exhibits a characteristic reflection at 2θ=21.3^o [2]. In the α-form, the molecular conformation is a fully extended planar zigzag, all-trans, and is packed in the more stable antiparallel-chain arrangement, whereas the γ-form adopts a helical or kinked structure and the parallel chain arrangement of hydrogen bonding, and thus is metastable [3]. It is generally believed that rapid crystallization favors the g-form and slow crystallization the α-form. Recently, Giller et al. [4] reported the role of solvent evaporation on the crystalline state of electrospun nylon-6 fibers. It was found that the formation of the metastable γ-form is due, in part, to the fast solvent-evaporation kinetics associated with the electrospinning process. Electrospinning is a simple and effective method for the production of nanostructured fibers (nanofibers) [5-7]. An electrostatically driven jet of polymer solution or melt induced by a high-voltage power supply is used to produce polymer fibers with diameters

ranging from a few micrometers to several nanometers. In general, electrospun nanofibers are randomly deposited onto the metal collector due to the bending instability associated with a charged jet [8]. Recently, there has been increased interest in well-aligned nanofibers for many applications, including electrical, optical, mechanical, and biomedical applications [9]. Up to now, various methods for macroscopically aligned electrospun fibers have been reported, such as using a high-speed rotating drum [10-12], a copper-wire drum [13], a scanning tip [14] or conductive plates containing an insulating gap [15, 16]. On the other hand, only a few studies on the molecular orientation of polymer chains in macroscopically aligned electrospun nanofibers have been published [12, 16-20]. Recently, we also reported that electrospun, macroscopically aligned, molecularly oriented nylon-6 nanofibers could be successfully prepared by controlling the linear velocity of a rotating collector as well as the gap of the negatively charged metal plates [16], as demonstrated by scanning electron microscopy (SEM) and polarized Fourier transform infrared (FTIR) spectroscopy. Such uniaxially oriented nanofibers exhibit a variety of potential applications in biomedicine, microelectronics, and electro-optics. In this paper, as an extension of our previous work, we study the effects of the gap size between the negatively charged metal plates on the macroscopic alignment, the molecular alignment and the crystal structure of the polymer chains in uniaxially aligned, electrospun nylon-6 nanofibers using SEM, polarized FTIR spectroscopy, and XRD, respectively.

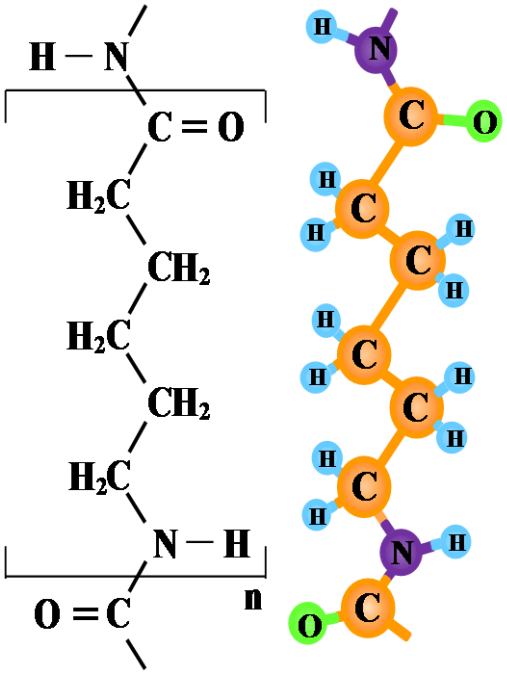

Figure 1 Chemical structure of nylon-6.

2.2 Experimental

2.2.1 Materials

Nylon-6 pellets were kindly supplied by Kolon Industries, Republic of Korea. The pellets were dried in an oven at 60 ^{o}C prior to use. The relative viscosity was measured using an Ubbelohde viscometer at room temperature, and its value was about 2.8, using H_2SO_4 as a solvent. Electrospinning was carried out using a nylon-6 solution concentration of 22 wt% in formic acid (98 %, containing 2 % water as a stabilizer), with an applied voltage of 13 kV and a tip-to-collector distance of 12 cm. To induce the uniaxial alignment of the nylon-6 nanofibers, a metal collector consisting of several metal plates separated by gap widths of 4, 8, and 12 mm was used. A schematic of the electrospinning apparatus used in this study is shown in Figure 2. Here, the parallel plates as an electrode stood on the silicon sheet as an insulator, and therefore the two electrodes were separated from each other. After electrospinning, the nylon-6 nanofibers were vacuum-dried to remove the residual solvents.

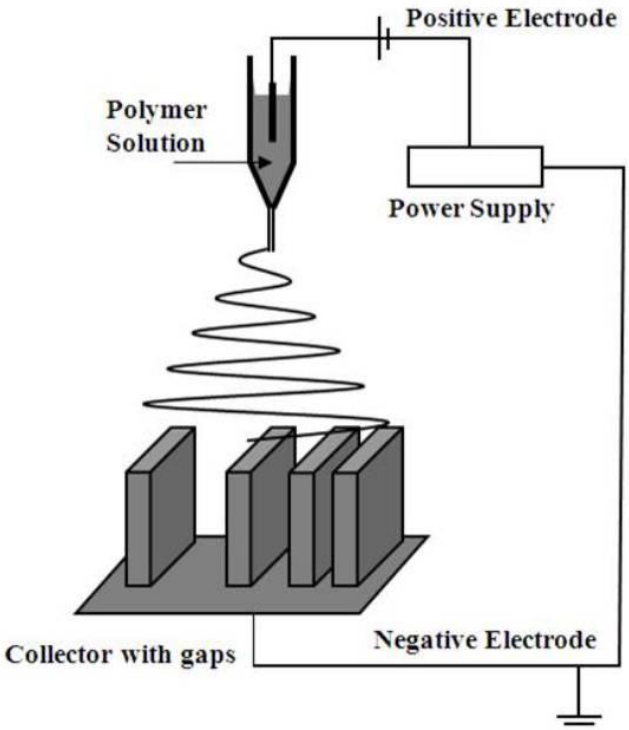

Figure 2 Schematic diagram of the electrospinning setup used in this study.

2.2.2 Characterization

The morphology of the electrospun nylon-6 nanofibers was examined using SEM (VE-8800, Keyence Co., Japan). To monitor the changes in the molecular orientation as a function of the gap size, an FTIR spectrometer (Nexus 670, Thermo Nicolet) with a ZnSe polarizer was used. The effective beam-spot size at the sample position of the microscope was measured to be $35\times12\mu m^2$ [full width at half maximum (FWHM)]. The spectra were recorded from 400 to $4000cm^{-1}$ with a resolution of 4 cm^{-1} and the coaddition of 128 scans. In parallel polarization, the direction of the oscillating electric field of the incident IR beam was parallel to the machine direction of the collection of the fibers (parallel to the fiber axis), while in perpendicular polarization it was perpendicular to the machine direction (perpendicular to the fiber axis).[16] In order to characterize the extent of uniaxial orientation in the uniaxially well-aligned, electrospun nylon-6 nanofibers produced using the different gap sizes, the dichroic ratio was calculated using the expression $R=P_{ll}/P_{\perp}$, where R is the dichroic ratio, P_{ll} is the parallel-polarized infrared-absorbance intensity and $P_{\perp}$ is the perpendicularly polarized infrared-absorbance intensity for a particular vibration in the observed FTIR spectra. The crystal structure of the electrospun nylon-6 nanofibers was evaluated using wide angle X-ray diffraction (WAXD, Rigaku Co., Japan) operating the diffractometer at 40 kV and 150 mA, using Cu Ka radiation. The scans were recorded over the range $2\theta=5\text{-}30^{o}$. The X-ray beam was controlled to be perpendicular to the aligned fiber axis in the uniaxially well-aligned, electrospun nylon-6 nanofibers.

2.3 Results and discussion

2.3.1 Morphologies

The electrospun nylon-6 nanofibers were collected onto the negatively charged metal plates, with the gap sizes of 4-12 mm between them, as a collector, which was able to induce a uniaxial alignment of the nanofibers. As shown in Figure 3, SEM images demonstrate that uniaxially well-aligned nylon-6 nanofibers (Figure 3a) were successfully formed in the gap of the negatively charged metal plates, and they had obviously different morphologies from the randomly oriented fibers (Figure 3b). This result agreed well with previous findings [16, 17], indicating that a stretching force was induced by the electrostatic potential which acted on the electrospun nanofibers across the gap during electrospinning. The surface morphology of the pure nylon-6 fibers was smooth and a narrow distribution of diameters was observed, with an average diameter of 330 nm. The diameters of the uniaxially aligned nanofibers were similar to those of the randomly deposited nanofibers, irrespective of the gap size. This means that there was no mechanical stretching effect in the uniaxially well-aligned nylon-6 nanofibers induced by the electrostatic force. This is in contrast to recent results that the average fiber diameter of aligned electrospun nanofibers produced using a high-speed rotating collector was decreased by increasing the speed of the rotating collector, because electrospun nanofibers were stretched and aligned by the mechanical-stretching forces during electrospinning.[17] Figure 4 shows the frequency distribution of angles, which shows the percentage of observations falling into each of several ranges of angle values, for the uniaxially aligned, electrospun nylon-6 nanofibers collected with gap sizes ranging from

4 to 12mm. On decreasing the gap size, the degree of alignment of the electrospun nylon-6 nanofibers was increased, presumably due to an enhanced electrostatic repulsive force across the gap. It is therefore expected that the longer the distance between the metal plates is, the lower the degree of fiber alignment should be, due to repulsive forces between the fibers giving rise to a disorder state of the fiber axis, as demonstrated by SEM analysis.

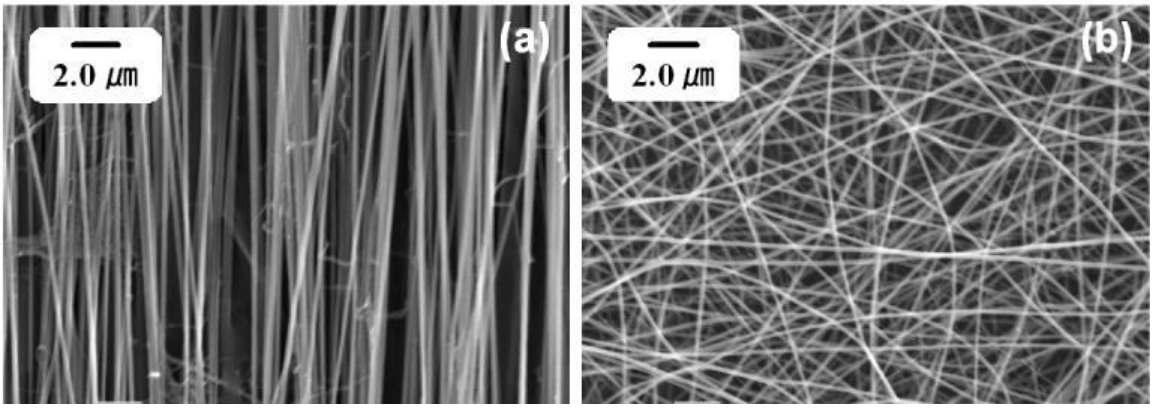

Figure 3 SEM images of: a) well-aligned nylon-6 nanofibers; b) randomly deposited nylon-6 nanofibers.

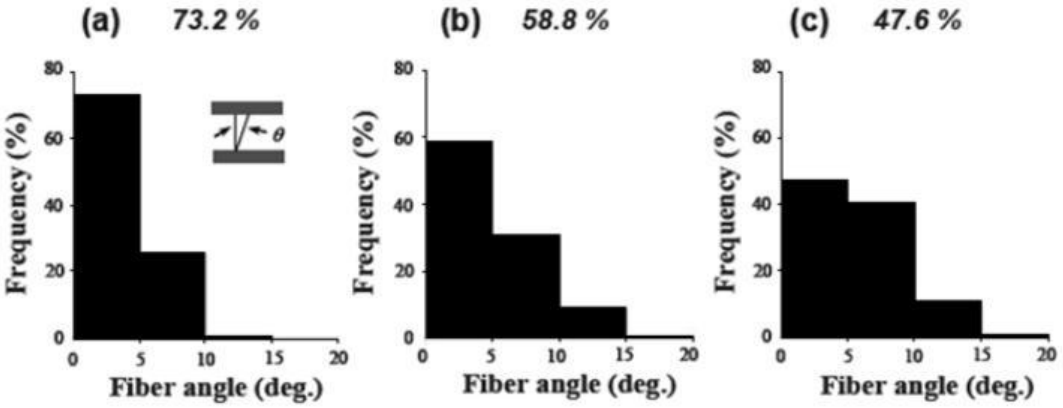

Figure 4 Frequency distribution of the electrospun nylon-6 nanofiber alignments: gap size of the charged metal plates: a) 4, b) 8, and c) 12mm. Here, the frequency distribution shows the percentage of observations falling into each of several ranges of angles.
The fiber angle is the angle (u) to the fiber axis, as shown in inset.

2.3.2 FTIR analysis

The molecular orientation in nanofibers and films has been analyzed using polarized FTIR spectroscopy [16, 17, 21]. Figure 5 shows polarized FTIR spectra of randomly collected and aligned electrospun nylon-6 nanofibers. The assignments of the IR bands for the nylon 6 were based on previously reported studies [17, 22, 23]. As expected, the parallel- and perpendicular-polarized FTIR spectra of the randomly distributed nylon-6 nanofibers were similar to each other (spectra A and B in Figure 5), suggesting that, if all the fibers were randomly oriented, the averaged degree of electrospun nylon-6 nanofiber alignment would yield a net-zero vector and result in no anisotropy. On the contrary, very different absorbance intensities, including for the NH-stretching (3300 cm^{-1}), and the amide I (1645 cm^{-1}), amide II (1544 cm^{-1}, primarily due to the carbonyl stretching vibration), and amide III (1367 and 1264 cm^{-1}) vibration bands were observed for the two polarized FTIR spectroscopy measurements, parallel and perpendicular to the nanofibers axis, for the uniaxially well-aligned nylon-6 nanofibers (spectra C and D in Figure 5). Compared to the randomly oriented nylon-6 nanofibers, the intensities of the amide II band at 1544 cm^{-1} (mainly attributable to C-N stretching and N-H in-plane bending) and the amide III band at 1367, 1264 and 1202 cm^{-1} in the parallel-polarized spectrum were increased (spectrum C in Figure 5). Moreover, as seen in Figure 6, it was clearly observed that the CO-NH in-plane vibration at 929 cm^{-1} attributed to the α-form exhibited a parallel direction (spectrum C in Figure 6), while the CO-NH in-plane vibration at 975 cm^{-1} attributed to γ-form crystals showed perpendicular polarization (spectrum D in Figure 6). These results indicate that there was a significant uniaxial orientation of the polymer chains in the uniaxially well-aligned, electrospun nylon-6

nanofibers collected between the charged parallel plates used as a collector, which also coincided well with previous results [16, 17].

Moreover, in the case of the uniaxially well-aligned, electrospun nylon-6 nanofibers, the parallel- and perpendicular- polarized FTIR spectra ranging from 1700 to 1500 cm^{-1} were investigated as a function of the width of the gap size between the metal plates. The results are shown in Figure 7. As the gap size between the metal plates increased, the intensity of the amide II band was relatively increased for the parallel polarization, while the intensity of the amide I band was relatively increased for the perpendicular polarization (Figure 7). A qualitative explanation may be as follows. Assuming that the molecular chains were aligned along the nanofiber axis in the uniaxially well-aligned nylon-6 nanofibers, one would expect that the carbonyl groups should be perpendicular to the fiber axis. Therefore, the absorption of the incoming parallel-polarized IR beam by the carbonyl groups would be minimal [24]. On the other hand, when the incident IR beam is perpendicular to the fiber axis, the amide I absorption attributed to the C-O bonds at 1645 cm^{-1} should reach a maximum, due to resonance between the carbonyl stretching and the electric field of the incoming polarized IR beam. When the molecular chains are parallel to the fiber axis, the amide II absorption should be maximum for the parallel polarization because the C-N stretching and N-H in-plane bending directions are almost parallel to the incident IR beam. In contrast, when the molecular chains are perpendicular to the fibers axis, the C-N stretching and N-H in-plane bending directions should be perpendicular to the incident IR beam, and therefore the amide II absorption should become weak for the parallel polarization. As a result, on increasing the gap size, the gradual increase of the amide II absorption and the gradual decrease of the amide I absorption upon an incident IR beam polarized parallel to

the fiber axis indicates that the molecular orientation to the fiber axis was relatively increased with increasing the gap size, and thereby resulted in an increased crystallinity. That is to say, a higher electric field strength during electrospinning can induce molecular orientation to the fiber axis, which is on the molecular scale and clearly different to the degree of fiber alignment. Thus, the shorter the distance between the metal plates is, the higher the electric-field strength applied to the uniaxially well-aligned electrospun nylon-6 nanofibers is, and thereby the molecular orientation and crystalline structures are affected, as demonstrated by the polarized FTIR spectroscopy and WAXD analyses. A similar such behavior was also observed in the perpendicular direction.

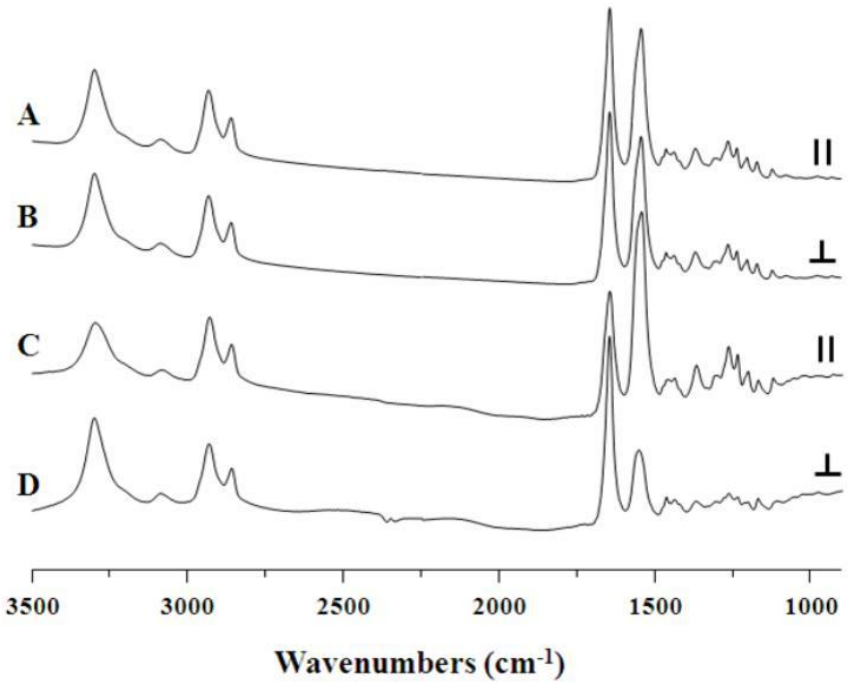

Figure 5 Polarized FTIR spectra of the electrospun nylon-6 nanofibers parallel (A) and perpendicular to the randomly deposited nanofibers (B); also shown are spectra for parallel (C) and perpendicular (D) to the axis of the macroscopically aligned nanofibers (gap size of 4 mm of the charged metal plates).

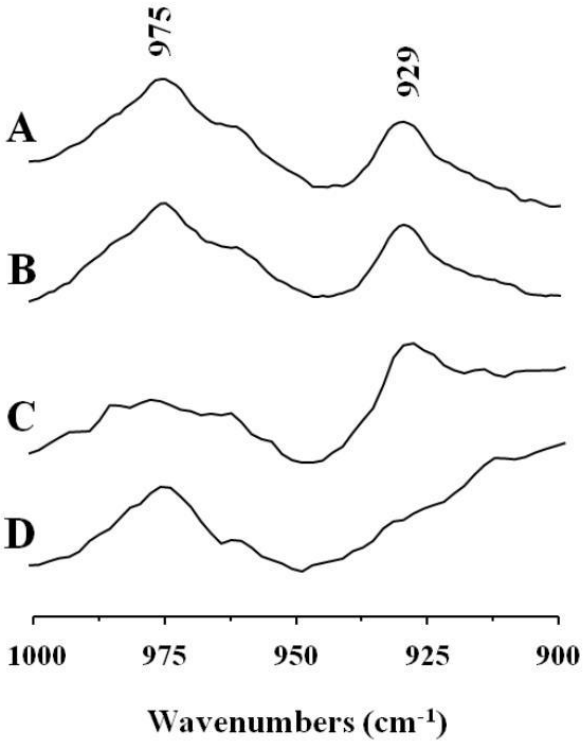

Figure 6 Polarized FTIR spectra of the electrospun nylon-6 nanofibers: parallel (A) and perpendicular polarization (B) of the randomly deposited nanofibers; and parallel (C) and perpendicular polarization (D) of the aligned nanofibers (void gap of 4 mm).

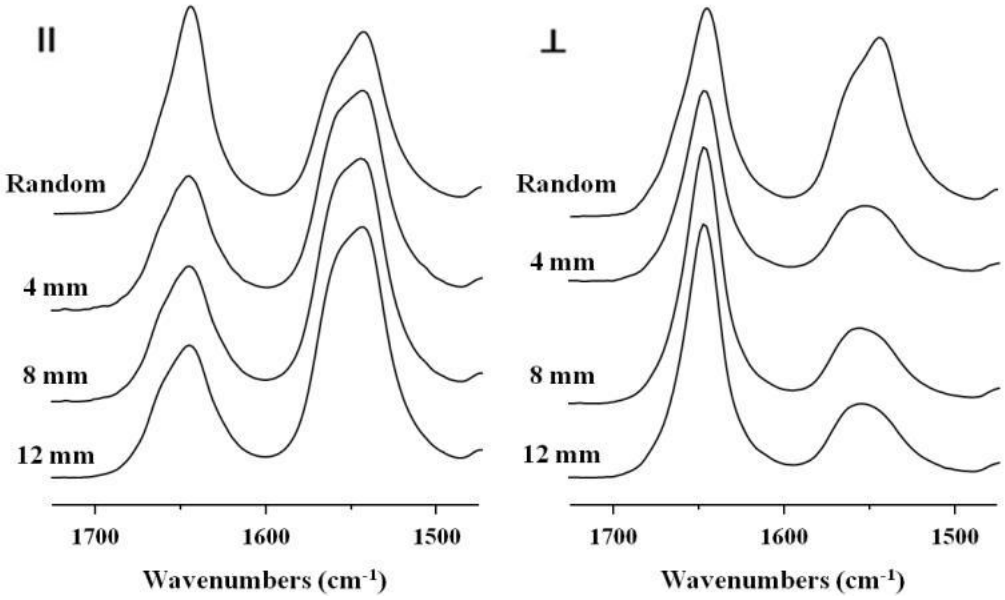

Figure 7 Polarized FTIR spectra of electrospun nylon-6 nanofibers: parallel (A) and perpendicular polarization (B).

2.3.3 WAXD analysis

Little is known about the crystalline structures (i.e., α- or γ-form) of nylon-6 and their transitions in electrospun nanofibers. Previous work by Murase and coworkers [25] showed that the macromolecular orientation and the crystalline structure of nylon-6 in conventional fibers depends on the fiber formation process, such as the take-up speed, with the γ-form predominant when the take-up speed is 6 km・min^{-1} and below, and the α-form predominant when the take-up speed is greater than 9 km・min^{-1}. Accordingly, it was expected that the crystal structure of the as-spun nylon-6 fibers could also depend markedly on the process conditions, such as the temperature, the humidity and the molecular weight. Here, the effect of the gap size on the crystal structure of the polymer chains in the uniaxially aligned, electrospun nylon-6 nanofibers was investigated. Figure 8 shows WAXD patterns of the as-spun nylon-6 nanofiber (A) and the uniaxially aligned, electrospun nylon-6 nanofibers collected on the metal plates with gap sizes of 4 (B), 8 (C), and 12 mm (D). As is evident in Figure 8, the as spun nylon-6 nanofibers display (001) diffraction peaks at 21.3^{o} (d-spacing.0.42 nm), characteristic of the γ-crystalline structure. The uniaxially aligned electrospun nylon-6 nanofibers show two diffraction peaks, (200) and mixed (002/202), at 20.3 and 23.7^{o} (d-spacing.0.44 and 0.38 nm, respectively), which are characteristic of the α-crystalline structure. The WAXD analysis indicates that the metastable γ-form was predominant in the as-spun nylon-6 nanofibers, and was transformed into the thermodynamically stable α-form by increasing the gap size, suggesting that the polymer chains were oriented parallel to the fiber direction in the uniaxially aligned, electrospun nylon-6 nanofibers, and thus that the molecular orientation to the fiber axis was enhanced on increasing the gap size. This result is crucial

and also coincided well with the polarized IR spectroscopy data.

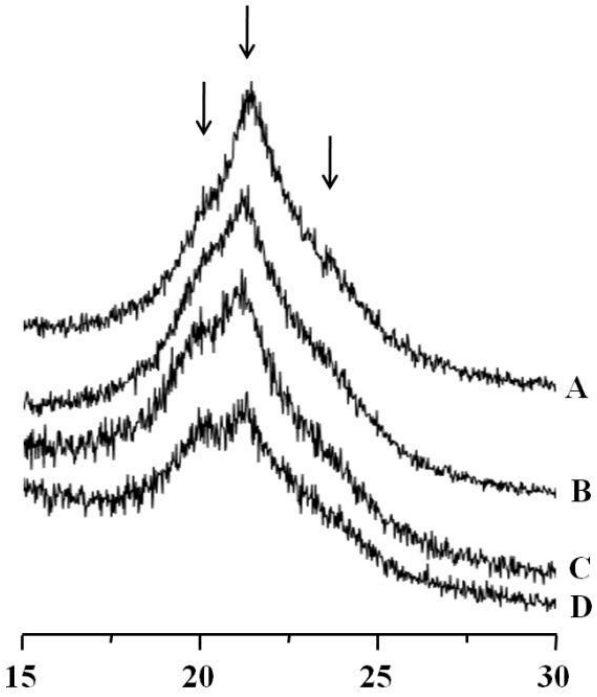

Figure 8 WAXD patterns of as-spun nylon-6 nanofibers (A) and the uniaxially aligned, electrospun nylon-6 nanofibers collected at the metal plates with gap sizes of: 4 mm (B), 8 mm (C), and 12 mm (D).

2.3.4 Dichroic ratios

The characterization of the molecular orientation for the well-aligned nylon-6 nanofibers could also be carried out through calculating the dichroic ratio of the different vibrational bands in the observed FTIR spectra. For the randomly deposited, electrospun nylon-6 nanofibers, the dichroic ratio was close to 1, indicating an equal IR absorbance intensity in the parallel and perpendicular directions. On the other hand, the dichroic ratio of the well-aligned nylon-6 nanofibers was different in some particular bands, indicating a change in the dipole moment of the particular bands in the parallel and perpendicular spectra and therefore in the polymer chains oriented along the nanofiber axis. Specifically, as the gap size increased, the amide II band (1544 cm^{-1}, mainly attributable to C-N stretching and N-H in-plane bending) and the CO-NH-CH_2 wagging (symmetry) at 1368 cm^{-1}, which was characteristic of the parallel polarization, and the C-C stretching band at 1121 cm^{-1}, characteristic of the amorphous phase, exhibited a larger dichroic ratio. These results suggest that the well-aligned nylon-6 nanofibers were more sensitive to parallel polarization, indicative of the preferred a-form by an increase in the gap size. The dichroic ratios of the IR bands from different vibrations are summarized in Table 1.

Table 1 Dichroic ratios of different vibrational bands of randomly deposited and well-aligned nylon 6 nanofibers electrospun using different gap sizes.

Wavenumber	Dichroic ratio			
cm^{-1}	Randomly deposited	Well-aligned (4 mm gap)	Well-aligned (8 mm gap)	Well-aligned (12 mm gap)
3 300	1.01	0.62	0.54	0.53
1 645	1.01	0.64	1.14	0.54
1 544	1.03	3.02	5.96	4.06
1 368	1.01	3.41	5.22	5.21
1 121	1.02	2.76	5.25	5.59

2.4 References

[1] M. Alger, Polymer Science Dictionary, 2nd ed. Chapman & Hall, London 1997.

[2] G. M. Kim, G. H. Michler, F. Ania, F. J. B. Calleja, Temperature dependence of polymorphism in electrospun nanofibres of PA6 and PA6/clay nanocomposites, Polymer 48 (2007) 4814-4823.

[3] A. Okada, M. Kawasumi, I. Tajima, T. Kuruachi, O. Kamigaito, A solid state NMR study on crystalline forms of nylon 6, J. Appl. Polym. Sci. 37 (1989) 1363-1371.

[4] G. B. Giller, D. B. Chase, J. F. Rabolt, C. M. Snively, Effect of solvent evaporation rate on the crystalline state of electrospun Nylon6, Polymer 51 (2010) 4225-4230.

[5] O. Ohsawa, K. H. Lee, B. S. Kim, S. Lee, I. S. Kim, Preparation and characterization of polyketone (PK) fibrous membrane via electrospinning, Polymer 51 (2010) 2007-2012.

[6] J. C. Park, T. Ito, K. O. Kim, K. W. Kim, B. S. Kim, M. S. Khil, H. Y. Kim, I. S. Kim, Electrospun poly(vinyl alcohol) nanofibers: Effects of degree of hydrolysis and enhanced water stability, Polymer J. 42 (2010) 273-276.

[7] C. K. Kim, B. S. Kim, F. A. Sheikh, U. S. Lee, M. S. Khil, H. Y. Kim, Amphiphilic Poly(vinyl alcohol) Hybrids and Electrospun Nanofibers Incorporating Polyhedral Oligosilsesquioxane, Macromolecules 40 (2007) 4823-4828.

[8] D. Li, Y. Xia, Electrospinning of Nanofibers: Reinventing the Wheel?, Adv. Mater. 16 (2004) 1151-1170.

[9] D. Li, Y. Wang, Y. Xia, Electrospinning of Polymeric and Ceramic nanofibers as Uniaxially Aligned Arrays, Nano Lett. 3 (2003) 1167-1171.

[10] J. A. Matthews, G. E. Wnek, D. G. Simpson, G. L. Bowlin, Electrospinning of Collagen Nanofibers, Biomacromol. 3 (2002) 232-238.

[11] W. E. Teo, M. Kotaki, X. M. Mo, S. Ramakrishna, Porous tubular structures with controlled fibre orientation using a modified electrospinning method, Nanotechnology 16 (2005) 918-924.

[12] J. H. Park, B. S. Kim, Y. C. Yoo, M. S. Khil, H. Y. Kim, Enhanced mechanical properties of multilayer nano-coated electrospun nylon 6 fibers via a layer-by-layer self-assembly, J. Appl. Polym. Sci. 107 (2008) 2211-2216.

[13] P. Katta, M. Alessandro, R. D. Ramsier, G. G. Chase, Continuous Electrospinning of Aligned Polymer Nanofibers onto a Wire Drum Collector, Nano Lett. 4 (2004) 2215-2218.

[14] J. Kameoka, R. Orth, Y. Yang, D. Czaplewski, R. Mathers, G. W. Coates, H. G. Craighead, A scanning tip electrospinning source for deposition of oriented nanofibers, Nanotechnology 14 (2003) 1124-1129.

[15] D. Li, Y. Wang, Y. Xia, Electrospinning Nanofibers as Uniaxially Aligned Arrays and Layer-by-Layer Stacked Films, Adv. Mater. 16 (2004) 361-366.

[16] M. V. Kakade, S. Givens, K. Gardner, K. H. Lee, D. B. Chase, J. F. Rabolt, Electric Field Induced Orientation of Polymer Chains in Macroscopically Aligned Electrospun Polymer Nanofibers, J. Am. Chem. Soc. 129 (2007) 2777-2782.

[17] K. H. Lee, K. W. Kim, A. Pesapane, H. Y. Kim, J. F. Rabolt, Polarized FT-IR Study of Macroscopically Oriented Electrospun Nylon-6 Nanofibers,

Macromolecules 41 (2008) 1494-1498.

[18] R. Jalili, M. Morshed, S. A. H. Ravandi, Fundamental parameters affecting electrospinning of PAN nanofibers as uniaxially aligned fibers, J. Appl. Polym. Sci. 101 (2006) 4350-4357.

[19] M. B. Bazbouz, G. K. Stylios, Alignment and optimization of nylon 6 nanofibers by electrospinning, J. Appl. Polym. Sci. 107 (2008) 3023-3032.

[20] L. M. Bellan, H. G. Craighead, Molecular orientation in individual electrospun nanofibers measured via polarized Raman spectroscopy, Polymer 49 (2008) 3125-3129.

[21] C. L. Hoffmann, J. F. Rabolt, Self-Assembled Thin-Film Blends by Polymer Codeposition: Poly(ethylene oxide) and Poly(methyl methacrylate), Macromolecules 29 (1996) 2543-2547.

[22] H. Arimoto, α–γ Transition of nylon 6, J. Polym. Sci., Part A 2 (1964) 2283-2295.

[23] N. Vasanthan, D. R. Salem, FTIR spectroscopic characterization of structural changes in polyamide-6 fibers during annealing and drawing, J. Polym. Sci., Part B: Polym. Phys. 39 (2001) 536-547.

[24] Y. Liu, L. Cui, F. Guan, Y. Gao, N. E. Hedin, L. Zhu, H. Fong, Crystalline Morphology and Polymorphic Phase Transitions in Electrospun Nylon-6 Nanofibers, Macromolecules 40 (2007) 6283-6290.

[25] S. Murase, M. Kashima, K. Kudo, M. Hirami, Structure and properties of high-speed spun fibers of nylon 6, Macromol. Chem. Phys. 198 (1997) 561-572.

Chapter 3

Improved the Mechanical properties of Isotactic poly (4-methyl-1-pentene) (PMP) fibrous Membrane Inducing Thermal-treatment and Stretching process

Chapter 3

Improved the mechanical properties of isotactic poly (4-methyl-1-pentene) (PMP) fibrous membrane inducing thermal-treatment and stretching process.

ABSTRACT

Isotactic poly (4-methyl-1-pentene) (PMP) is one of the polyolefin is used a wide range of applications. Electrospinning technique has a particular fascination for fabricating nanofibers, and the electrospun PMP nanofibers have long been of interest in various fields. In spite of their significance, polyolefin including PMP is highly insoluble in organic solvents due to their high chemical resistance and electrical resistivity, therefore, electrospinning of these polyolefin is not viable. In this study, morphology of electrospun PMP fibrous membrane with thermal-treatment and stretching process were investigated by SEM. The thermal-treated and stretched, post-treated, electrospun PMP membrane had a uniaxially arrangement with bonding points between fibers. Crystallinity of the post-treated electrospun PMP fibers increased greatly more than 10% by calculated DSC data. It is also confirmed that crystalline structure of post-treated PMP fibers changed from form-II to stable form-I by using WAXD. As a result, we succeeded in improving mechanical property of PMP fibrous membrane by heat-stretching due to inducing the increase of crystallinity, which exhibited around 4.1 times higher tensile strength and 14.1 times higher Young's modulus than pure PMP fibrous membrane.

3.1 Introduction

Electrospinning is one of the very simple and highly versatile techniques for fabrication of nanofiber. In fact, this method has significant advantages such as capability of successive spinning, relative ease, and straightforward approach for fabricating nanofibers when compared to other conventional techniques. Nanofiber produced by electrospinning has received a great deal of attention in recent years, and the nanofiber materials have been used in various fields such as medical [1], electrical [2], filter [3], and electronics device [4]. Owing to the importance of these nanofiber materials, the development of nanofiber mass production *via* electrospinning has been widely focused by many researches. Electrospun nanofiber membrane has many excellent properties such as high-specific surface area and large pore size. However, due to low density, the mechanical properties of these nanofibers are exceptionally-low, and therefore, the commercial viability is highly limited. Well known that, thermal-treatment technique is a reliable method for improving the mechanical properties of electrospun fibrous membrane, because the thermal-treatment technique can induce the change of crystalline structure and removal residual solvent of the fibers membrane [5, 6]. Hou *et al*., [7] investigated the characteristic of stretching-induced electrospun PAN nanofiber membranes incorporated carbon nanotubes (CNTs). They found that the heat-stretching process play an effective role on the mechanical properties of the nanofibers by changing its crystalline state and morphology.

Polyolefin such as polyethylene (PE), polypropylene (PP), and poly (4-methyl-1- pentene) (PMP) is used in a wide range of applications. However, polyolefin including PMP is highly insoluble in organic solvents owing to their high

chemical resistance and electrical resistivity and, therefore, electrospinning of these polyolefin is not feasible. Meanwhile, Lee *et al*., [8] reported that the isotactic PMP fibrous membranes could be successfully prepared from the solution of solvent and non-solvent mixture by solution electrospinning. They have clarified the relationship between the morphological appearance of PMP fibrous and the solvent and/or non-solvent used to electrospun them. Later, Lee *et al*., [9] investigated the crystallization behavior of electrospun poly(1-butene) (PB)/PMP blend fibrous membranes. They concluded that the PMP component of the blend polymer is affected due to the wide disparity of the melting temperatures and crystalline structures of the blend components. In fact, the PMP has a complex polymorphic and many characteristics behaviors such as high optical transparency due to the similar densities between its crystalline (0.813 g/cm^3) and amorphous regions (0.830 g/cm^3), excellent dielectric properties, high chemical resistance and high permeability to gases [10, 11]. Despite the existence of such a great properties, to the best of our knowledge, there are only two reports [8, 9] about electrospun PMP fibrous membranes.

Therefore, the purpose of this work is study on the special characteristic of electrospun PMP fibrous membrane using thermal-treatment and heat-stretching technique. Particularly, we have investigated the effect of the morphology of PMP fibers, change in the crystalline structure, and mechanical properties by inducing thermal-treatment.

3.2 Experimental

3.2.1 Materials

Isotactic poly (4-methyl-1-pentene) (PMP) with a melt index of 26.00 g/10 min (260 ^{o}C/5 kg, ASTM-D1238), cyclohexane, acetone, and dimethylformamide (DMF) were purchased from Sigma Aldrich and used as received. PMP was dissolved in a mix solution of cyclohexane, acetone, and DMF at facultative mixing ratios at 60 ^{o}C with the help of a magnetic stirrer for 12 h until a homogeneous solution was obtained. After cooling to 30 ^{o}C, the resultant solution was used for electrospinning.

3.2.2 Preparation of the electrospun PMP fibrous membranes and thermal-treatment and stretching process

The electrospinning were performed as per our previous reports [12-14]. The solution was poured into a plastic syringe connected with a 20 G capillary metal tip in which there was a copper wire as an electrode, the drum collecting roller was placed at a distance of 15 cm from the capillary metal tip and a voltage of 18 kV was applied by a high voltage power supply (HAR-100*12, Matsusada. Co., Japan).

Prepared electrospun PMP fibrous membranes were thermal-treated in an electrical furnace at 180 and 220 ^{o}C. Additionally, a PMP fibrous membrane was heat-stretched at 180 ^{o}C. In the typical procedure, both sides of the PMP fibrous membrane were clipped with rectangle ceramics. Then, one side was hooked from the ceiling of the electrical furnace and the other side was loaded 15 N/m^2 using metal weight to be tension

with for 2 h to stabilize at 180 ^{o}C. For convenience, thermal-treated PMP fibrous membranes at 180 and 220 ^{o}C, and heat-stretched PMP fibrous membrane at 180 ^{o}C are denoted as PMP-180, PMP-220 fibrous membrane and PMP-180st fibrous membranes, respectively.

3.2.3 Characterization

The morphologies of electrospun pure PMP fibrous membranes, PMP-180, PMP-220, and PMP-180st samples were examined with scanning electron microscope (SEM, JSM-5300, JEOL Ltd., Japan).

The thermal property of the each treated electrospun PMP fibrous membrane was investigated by DSC (Thermo plus DSC 8230, Rigaku Co., Japan) by heating from 30 to 250 ^{o}C under a continuous nitrogen purge of 50 mL/min; the heating rate was 10 ^{o}C /min.

The prepared each electrospun PMP fibrous membrane was subjected to X-ray diffraction (WAXD, X-ray Diffractometer, Rigaku Co., Japan), for investigating the change of crystalline structure, operating at 40 kV and 150 mA using Cu Kα radiation, and scan were recorded over 2θ range of 5-25^{o}.

The mechanical behaviors of each electrospun PMP fibrous membrane was determined by using a universal testing machine (TENSILON RTC1250A, A&D Company Ltd., Japan) under a crosshead speed of 10 mm/min at ambient temperature (T=23-25 °C). In accordance with ASTM D-638, samples were prepared in the form of a dumbbell-shape. The tensile modulus, tensile strength, and elongation at break were obtained from the stress-strain curves.

3.3 Results and discussion

3.3.1 Morphologies

PMP is highly soluble in cyclohexane though it has high chemical resistibility, but this solvent has drawbacks such as low-volatility and -polarity. Lee *et al*. [8] used cyclohexane/acetone/DMF (80/10/10, w/w/w) mixture to increase the volatility and polarity of the PMP solution for electrospinning. They found that the spinnability of the PMP fibers is improved; however, there are many beads are observed. In order to overcome this drawback, in the present study, mixture ratio of cyclohexane/acetone/DMF to prepare PMP solution was investigated in detail. The mixture ratios of cyclohexane/acetone/DMF were 80/15/5, 80/10/10, 80/5/15, and 80/0/20 (w/w/w). Fig. 1 shows the SEM images of the electrospun PMP fibers produced by the different solvent ratios of cyclohexane/acetone/DMF. When the solvents comprised of a mixture of cyclohexane/acetone/DMF, 80/15/5 (w/w/w) were used, there were many large beads observed on the PMP fibrous membrane which might be due to poverty of DMF, and inducing a low-polarity. In comparison to 80/15/5 (w/w/w) ratio, the 80/10/10 (w/w/w) mixture ratio is better as very less beads are observed; this is because the polarity of the PMP solution increased. Furthermore, by increasing the DMF ratio of the mixed solvents [80/5/15 (w/w/w)], beads on the electrospun PMP fibers were disappeared, and the fiber diameter substantially decreased. It is considered that the relation of volatilization and polarity bring a balance at this mixture solvents ratio. Finally, a mixture solvent of 80/0/20 (w/w/w) was used for the formation of electrospun PMP fibers, a lot of beads attributed to the polarity of PMP solution, but PMP fibers were formed without volatility

of solvents because of the high boiling temperature of the DMF. Based on the results obtained a mixture solvent of 80/5/15 (w/w/w) was decided as an optimum for the production of continues and bead free electrospun PMP fibrous membrane.

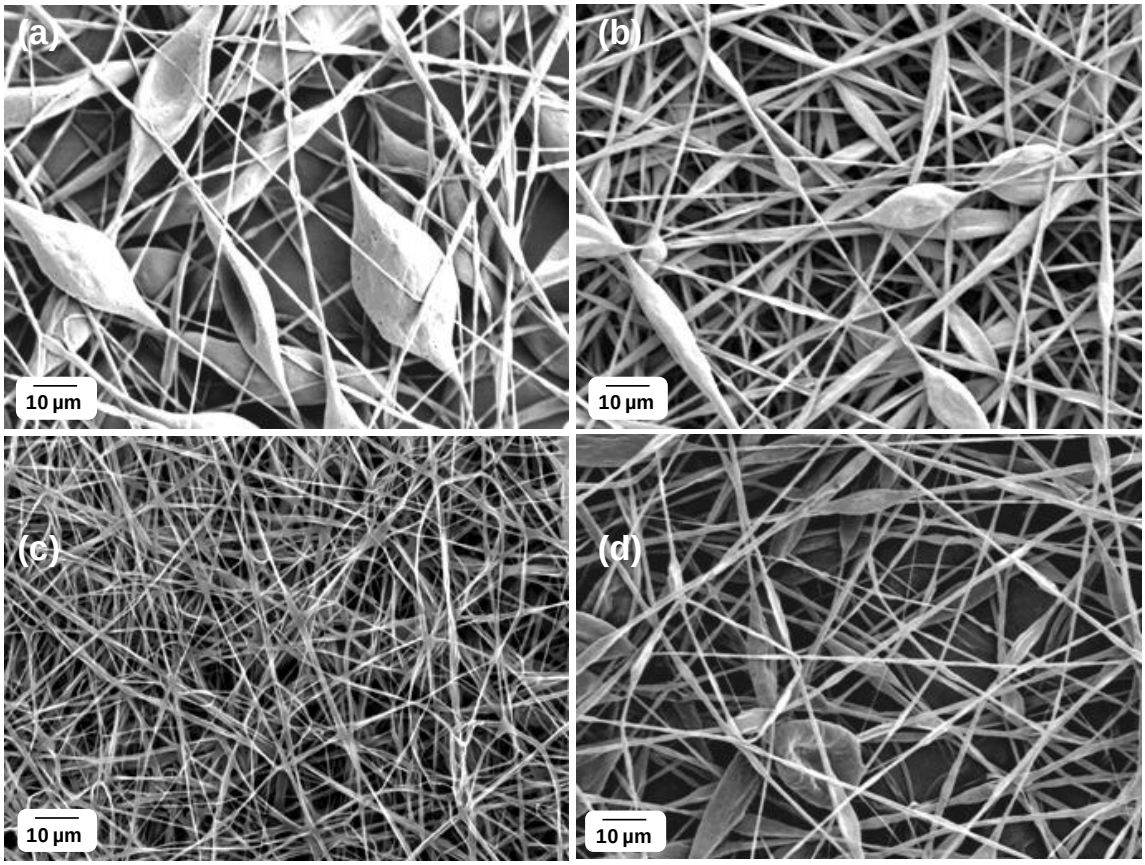

Figure 1 SEM images of electrospun PMP fibers produced by each mixture solvent ratios of cyclohexane/acetone/DMF; (a) 80/15/5, (b) 80/10/10, (c) 80/5/15, (d) 80/0/20.

Figure 2 shows SEM images of the thermal-treated electrospun PMP fibers produced by a mixture solvent of cyclohexane/acetone/DMF, 80/5/15 (w/w/w). As can be seen in Fig. 2a, most of the thermal-treated electrospun PMP fibers at 180 ^{o}C (PMP- 180) were crinkly cause of thermal shrinkage, and the pores in the nanofiber membrane reach a large size. Then, when the temperature increased to 220 ^{o}C which is close to melting point of PMP (235 ^{o}C), it is confirmed that crinkly fibers disappear and there exists many bonding points between the fibers (PMP-220, Fig. 2b). The slight surface dissolvable of PMP fibers produced in joint welding of the fibers at their proximate points. Then, the electrospun PMP fibrous membrane was thermal-treated at 180 ^{o}C with stretching (PMP-180st) process. In fact, the softening temperature of PMP was 178 ^{o}C (ASTM D 1525). The fibers are stretched by giving a force of 15 N/m^2 using metal weight in the boom of the fiber membrane. The arrows in Fig. 2 c and d show the stretching direction. As can be seen from Fig. 2c, the fibers have a uniaxial arrangement with bonding points between fibers. By means of load to PMP fibrous membrane on the PMP softening temperature, the PMP fibers were extended easily and highly. Over the thermal-treatment temperature at 180 ^{o}C, morphology of PMP fibers was unsustainable and PMP fibrous membrane changed like a film state (Fig. 2d) or the PMP fibrous membrane fractured without taking a load.

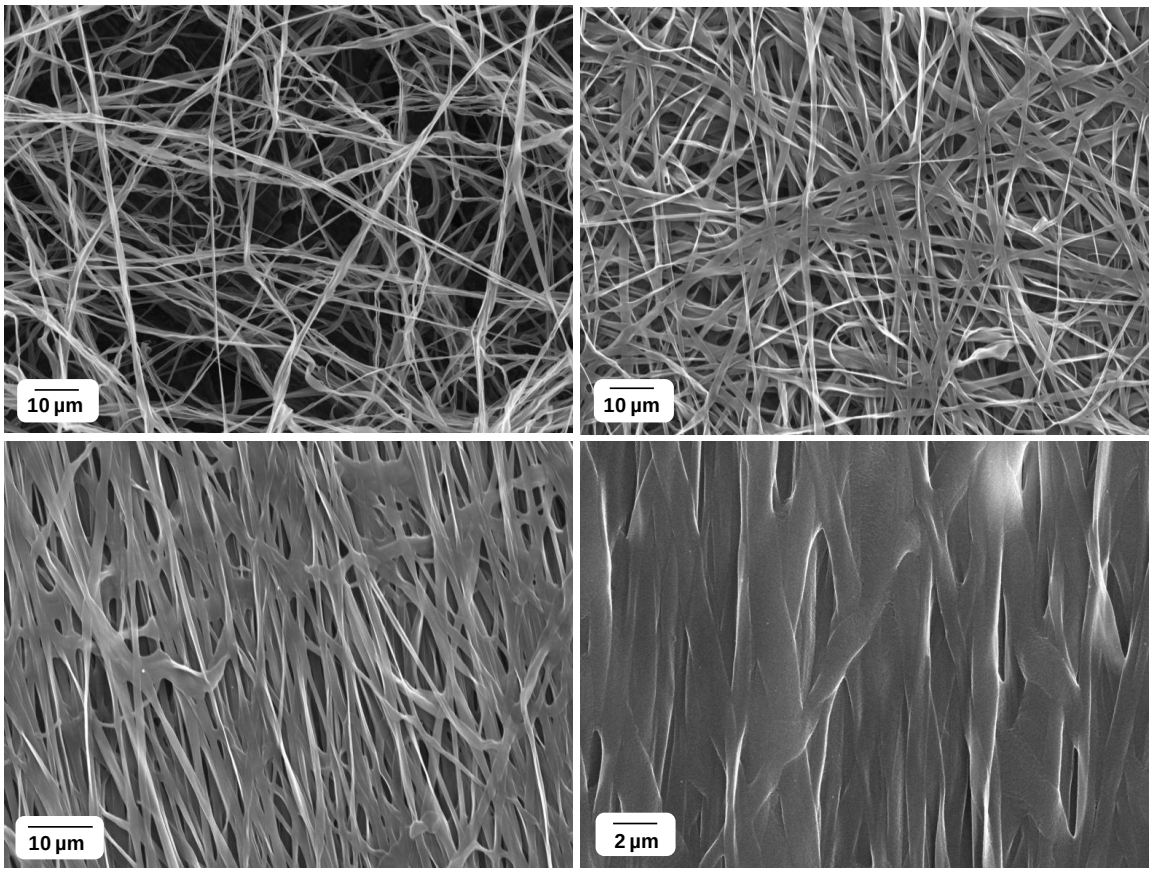

Figure 2 SEM images of Thermal-treated electrospun PMP fibers produced by mixture solvents of cyclohexane/acetone/DMF, 80/5/15 (w/w/w); (a) thermal-treated at 180 ^{o}C, (b) thermal-treated at 220 ^{o}C, (c) thermal-treated at 180 ^{o}C with stretching process, and (d)thermal-treated at 200 ^{o}C with stretching process.

3.3.2 DSC analysis

The crystallization behavior of thermal-treated electrospun PMP fibers was investigated by using DSC. Figure 3 shows DSC thermograms of electrospun PMP fibers with thermal-treatment by different temperatures and stretching process. The melting temperatures (235 ^{o}C) of electrospun PMP fibers after thermal-treatment and stretching process have not changes compared to electrospun pure PMP fibers. However, the shapes of endothermic peak are obviously different in appearance, and by increasing thermal-treatment temperature and stretching process, the shape of endothermic peak became sharper and sharper. The degree of crystallinity of the electrospun PMP fibers can be estimated by integrating the melt endotherm (heat of fusion, ΔH_f) and calculating the ratio with that (ΔH_f^0) of a theoretical 100% crystalline PMP. A ΔH_f^0 value of 61.7 J/g was used to calculate the degree of crystallinity of the electrospun PMP fibers [15]. The calculated crystallinity values of the electrospun pure PMP, PMP-180, PMP-220, and PMP-180st fibers were found to be 26.4, 31.3, 32.6, 37.3 %, respectively. For all three thermal-treated samples, an increase of the degree of crystallinity was observed compared to the electrospun pure PMP fibers. It is particularly worth noting that the degree of crystallinity of PMP-180st is greatly high by inducing stretching process during thermal-treatment.

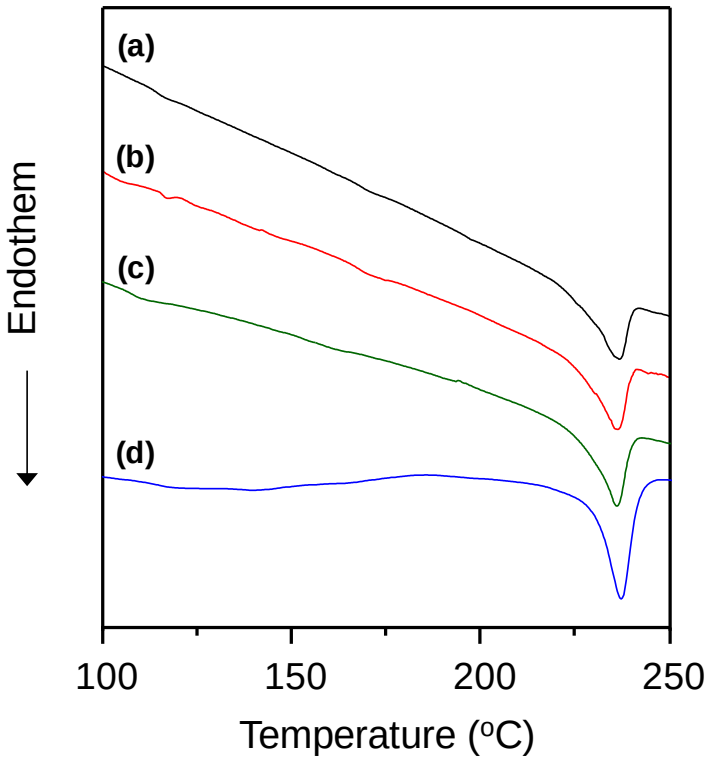

Figure 3 DSC data for electrospun PMP fibers; (a) pure, (b) thermal-treated at 180 ^{o}C, (c) thermal-treated at 220 ^{o}C, and (d) thermal-treated at 180 ^{o}C with stretching process.

3.3.3 WAXD nanlysis

Figure 4 presents WAXD patterns of electrospun pure PMP, PMP-180, PMP-220, and PMP-180st fibers. Five different crystalline forms have been found for PMP [16]. It is well-known that form I is the most stable crystalline form that occurs in formation of the fibers by extruding process frequently. The diffractive peak of electrospun pure PMP fibers shows crystalline form-II in Figure 4(a) [17] for the season that the stretching process does not exist from polymer solution to fiber formation during electrospinning process. Rosa et al. reported that form-II, III, and IV of PMP crystalline forms transformed into form-I of the stable crystalline form with increase temperature [18]. In this study, it is confirmed that thermal-treated electrospun PMP fibers (PMP-180 and PMP-220) transformed from form-II to form-I as can be seen in Figure 4 b and c, and the specific peaks of around 9.2^{o}, 13.1^{o}, 16.3^{o}, 18.1^{o}, 21.1^{o}, and 22.0^{o} corresponding to (200), (201), (212), (321), (400), and (203) crystallographic planes of stable form-I orthorhombic phase [16, 19, 20]. The specific peak intensities are sharply and strongly with increasing thermal treatment temperature. In Figure 4(d), it would appear that electrospun PMP-180st forms the crystalline form-I as well as PMP-180 and PMP-220, but the peaks around 16.3^{o} and 18.1^{o} are greatly decreased, and that of 13.1^{o} and 21.1^{o} are powerfully increased. The diffractive peak of PMP-180st fiber is extremely sharp and has very high intensity because of heat-stretching process which contributes to the crystalline development. This result is significant and also coincided well with above DSC result.

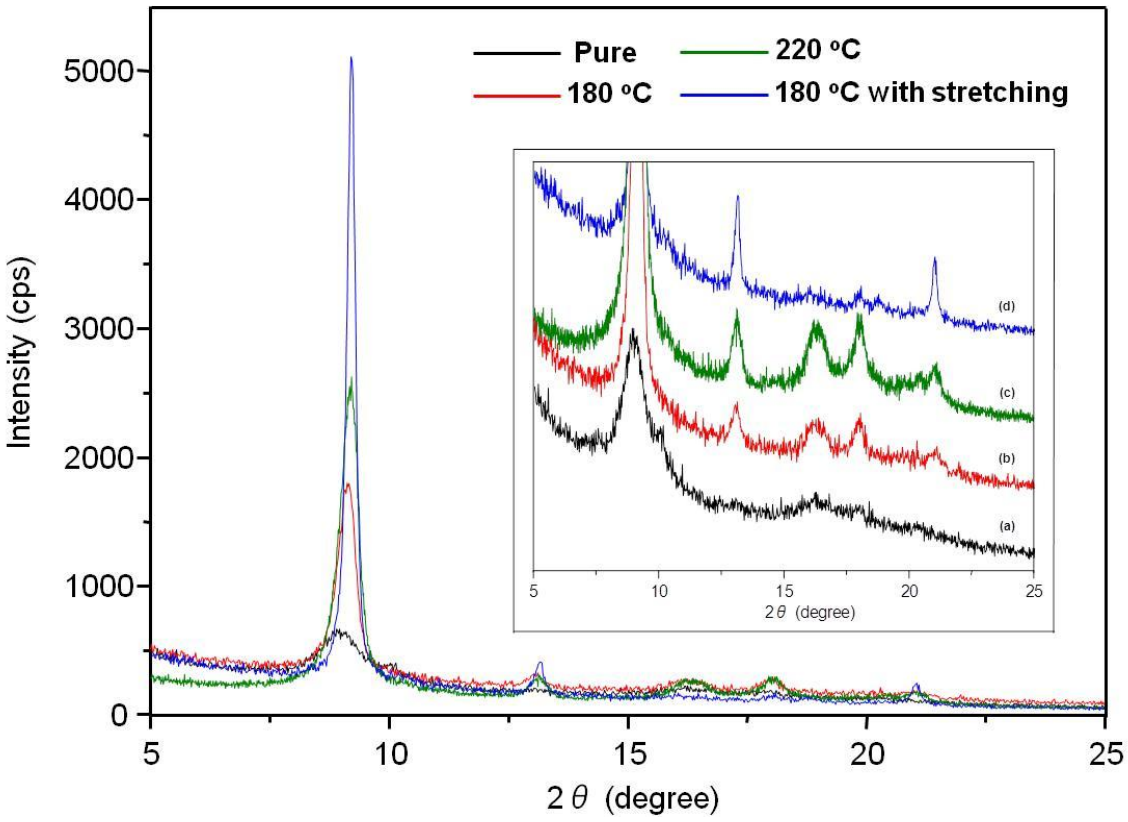

Figure 4 WAXD patterns of electrospun PMP fibers; (a) pure, (b) thermal-treated at 180 °C, (c) thermal-treated at 220 °C, and (d) thermal-treated at 180 °C with stretching process.

3.3.4 Mechanical properties

Figure 5 shows typical stress-strain curves of the electrospun pure PMP, PMP-180, PMP-220, and PMP-180st fibrous membranes. PMP-180 and -220 fibrous membranes produced by thermal-treatment were superior in terms of the mechanical properties, all of tensile strength, elongation, and Young's modulus (b and c in Fig. 5). The electrospun PMP-180 and -220 fibrous membrane has 16.47 and 17.58 MPa, 60.6 and 55.1 %, and 147.83 and 226.09 MPa corresponding to each tensile strength, elongation, and Young's modulus, respectively. It is also considered that a higher thermal-treatment temperature meant higher tensile strength and Young's modulus because the crystalline form of PMP fibers changed from unstable form-II to stable crystalline form-I as can be seen in above WAXD, and the crystallinity of PMP fibers has increased as can be expected from the results of DSC and WAXD. Additionally, they showed greater elongation at break than pure PMP fibrous membrane (Fig. 5a) due to occurring in thermal contraction and crinkly. Furthermore, PMP-180st fibrous membrane (Fig. 5d) prepared by thermal-treatment at 180 oC and stretching process was pulled to the extended direction by applied load, and this sample exhibited around 4.1 times higher tensile strength and 14.1 times higher Young's modulus than pure PMP fibrous membrane because the crystallinity of PMP fibers was induced by thermal-treatment and stretching process, and the crystalline form of PMP fibers became specific form-I structure as can be seen in the result of WAXD. It is confirmed that the mechanical strength of electrospun PMP fibrous membrane was successfully improved by means of thermal-treatment and stretching process.

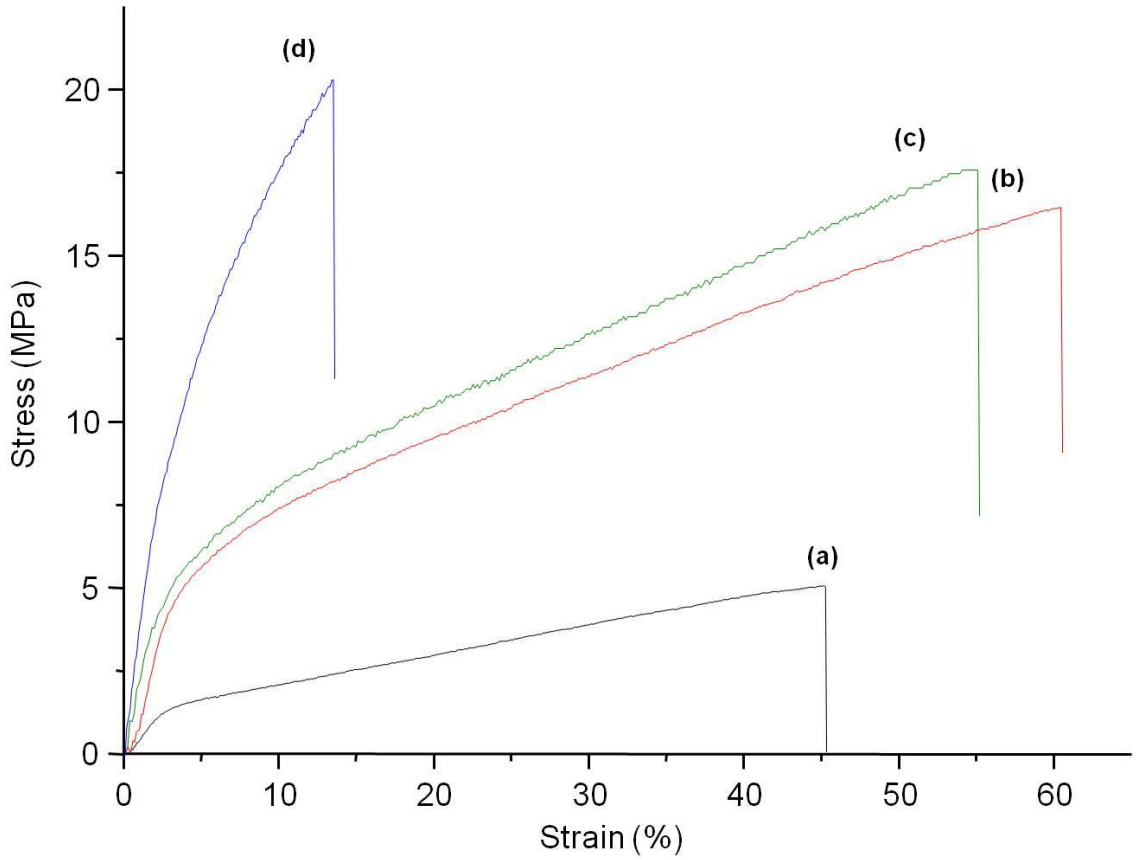

Figure 5 Stress-Strain curves for e electrospun PMP fibers; (a) pure, (b) thermal-treated at 180 ^{o}C, (c) thermal-treated at 220 ^{o}C, and (d) thermal-treated at 180 ^{o}C with stretching process.

3.4 References

[1] N. Reddy, H. Xu, Y. Yang, Unique Natural-Protein Hollow-Nanofiber Membrane Produced by Weaver Ants for Medical Applications, Biotechol. Bioeng. 108 (2011) 1726-1733.

[2] R.M. Robert, M.G. Betar, V.T. Carl and S.H. Yang, All-carbon-nanofiber electrodes for high-energy rechargeable Li-O_2 batteries, Energy Environ. Sci. 4 (2011) 2952-2958.

[3] S. Wannes, Z. martin, K. Dusan, 3D modeling of filtration process via polyurethane nanofiber based nonwoven filters prepared by electrospinning process. Chem. Eng. Sci. 66 (2011) 613-623.

[4] Z.M. Huang, Y.Z. Zhang, M. Kotaki, S. Ramakrishna, A review on polymer nanofibers by electrospinning and their applications in nanocomposites. Comp. Sci. Technol. 63 (2003) 2223-2253.

[5] Y. You, S.W. Lee, S.J. Lee, W.H. Park, Thermal interfiber bonding of electrospun poly(L-lactic acid) nanofibers, Mater. Lett. 60 (2006) 1331-1333.

[6] H.A. Tsai, Y.S. Ciou, C.C. Hu, K.R. Lee, D.G. Yu, J.Y. Lai, Heat-treatment effect on the morphology and pervaporation performances of asymmetric PAN hollow fiber membranes, J. Membr. Sci. 255 (2005) 33-47.

[7] X. Hou, X. Yang, L. Zhang, E. Waclawik, S. Wu, Stretching-induced crystallinity and orientation to improve the mechanical properties of electrospun PAN nanocomposites, Mater. Des. 31 (2010) 1726-1730.

[8] K.H. Lee, S. Givens, D.B. Chase, J.F. Rabolt, Electrostatic polymer processing of isotactic poly(4-methyl-1-pentene) fibrous membrane, Polym. 47 (2006)

8013-8018.

[9] K.H. Lee, S.R. Givens, C.M. Snively, B. Chase, J.F. Rabolt, Crystallization Behavior of Electrospun PB/PMP Blend Fibrous Membranes, Macromol. 41 (2008) 3144-3148.

[10] J.A. Griffith, B.G. Rndby, Dilatometric measurements on poly(4-methyl-1-pentene) glass and melt transition temperatures, crystallization rates, and unusual density behavior, J. Polym. Sci. 44 (1960) 369-381.

[11] D.R. Panse, P.J. Phillips, Polymer data handbook. New York: Oxford University Press Inc. (1999) 658e63.

[12] O. Ohsawa, K. H. Lee, B. S. Kim, S. Lee, I. C. Kim, Preparation and characterization of polyketone (PK) fibrous membrane via electrospinning, Polym. 51 (2010) 2007-2012.

[13] N. Kimura, H. K. Kim, B. S. Kim, K. H. Lee, I. S. Kim, Molecular Orientation and Crystalline Structure of Aligned Electrospun Nylon-6 Nanofibers: Effect of Gap Size, Macromol. Mater. Eng. 295, (2010) 1090-1096.

[14] B.S. Kim, I.S. Kim, Recent Nanofiber Technologies: A Perspective for a Special Issue of Polymer Reviews, Polym. Rev. 51 (2011) 235-238.

[15] H.J. Hayes, T.J. McCarty, Maleation of Poly(4-methyl-1-pentene) Using Supercritical Carbon Dioxide, Macromol. 31 (1998) 4813-4819.

[16] G. Charlet, G. Delmas, Effect of solvent on the polymorphism of poly(4-methylpentene-1): 2. Crystallization in semi-dilute solutions, Polym. 25 (1984) 1619-1625.

[17] C.D. Rosa, Crystal Structure of Form II of Isotactic Poly(4-methyl-1-pentene), Macromol. 36 (2003) 6087-6094.

[18] T. Miyoshi, O. Pascui, D. Reichrt, Large-Amplitude Motions of Form III of Isotactic Poly(4-methyl-1-pentene) Crystallites Prior to Crystal-Crystal Transformation, Macromol. 37 (2004) 6653-6656.

[19] S. Chen, J. Jin, J. Zhang, Non-isothermal crystallization behaviors of poly(4-methyl-pentene-1), J. Therm. Anal. Calorim. 103 (2011) 229-236.

[20] S.M. Aharoni, G. Charlet, G. Delmas, Investigation of Solutions and Gels of Poly(4-methyl-1-pentene) in Cyclohexane and Decalin by Viscosimetry, Calorimetry, and X-ray Diffraction. A New Crystalline Form of Poly(4-methyl-1-pentene) from Gels, Macromol. 14 (1981) 1390-1394.

Chapter 4

Effects of Fe^{2+} ions on morphologies, microstructures and mechanical properties of electrospun nylon-6 nanofibers

Chapter 4

Effects of Fe^{2+} ions on morphologies, microstructures and mechanical properties of electrospun nylon-6 nanofibers

ABSTRACT

In this study, nylon-6 nanofiber mats containing Fe^{2+} ions were fabricated via electrospinning. The resultant electrospun nylon-6/$FeCl_2$ nanofiber mats were characterized by SEM, TEM, Fourier transform IR spectroscopy, wide angle XRD and DSC. Unique morphological features, such as spider's-web-like morphologies, were observed and became evident with increasing additive Fe^{2+} ions. The metastable γ form was predominant in the as-spun nylon-6 nanofibers. The relative intensity of such γ form gradually decreased with increasing additive Fe^{2+} ions, indicative of transformation of the crystalline structure in the electrospun nylon-6/$FeCl_2$ nanofibers due to strong molecular interactions between the nylon-6 backbone and the additive Fe^{2+} ions. The effects of additive Fe^{2+} ions on the mechanical properties of both nonwoven nanofiber mats and single nanofibers were investigated. In particular, Young's modulus of nylon-6/$FeCl_2$ single nanofibers gradually increased from 1.46 to 5.26 GPa with increasing additive Fe^{2+} ions.

4.1 Introduction

Recently, there has been an increasing interest in new research subjects in nanomaterials science. In particular, nanofibers and nanotechnology in textiles have attracted a great deal of attention from various applications, such as electrical, biomedical and protective products [1-3]. A useful method of nanofiber production is now well known as electrospinning, thanks to the relative ease and inexpensive and straightforward method of fabricating nanofibers compared with other techniques, e.g. drawing [4], template synthesis [5, 6], self-assembly [7-9], and phase separation [10]. Electrospinning is a fiber spinning technique driven by a high voltage source using a polymeric solution or melt that can produce polymer fibers with diameters ranging from several microns to nanometers [11-13]. The fascinating advantages of nanotechnology have engendered a renewed attention to this convenient and economical technology, which enables engineers to produce nanofibers suitable for the creation of numerous technologically excellent candidates for applications in filtration [14], protective textiles [3], reinforcement in composite materials [15], catalysis [16], sensors [17] as well as biomaterials for wound devices [18] and drug delivery and scaffolds in tissue engineering [19, 20]. It is well known that nylon-6 exhibits crystalline structures of two different types, α- and γ-forms, and is one of the most commonly used polymers. The α-form is a fully extended planar zigzag conformation and is thermodynamically stable [21, 22]. In contrast, in the γ-form the molecular conformation is a helix structure, which is metastable[23, 24]. All nylon-6 amide bonds lie in the same direction. The α- and γ-crystal forms are known to be changed by chemical and physical mechanisms such as high-speed spinning [25-27], nanocomposite containing clay [28, 29], carbon nanotubes

[30] and additives [31] etc. The tuning of such α- and γ-crystal forms is very important because their different structures impart different physical and mechanical properties. For instance, Young's modulus of the α-crystal form is higher than that of the γ-crystal form. Also, the γ-crystal form has been noted to predominate in melt-spun nylon-6 fibers and nylon-6/clay nanocomposites [32, 33]. It is generally believed that rapid crystallization favors the γ-crystal form and slow crystallization favors the α-crystal form [28]. In our previous work [34], we studied the effect of the gap size on the molecular orientation and crystalline structure of uniaxially well-aligned nylon-6 nanofibers produced in the gap between negatively charged metal plates. We found that the metastable γ-crystal form was predominant in as-spun nylon-6 nanofibers and was transformed into the thermodynamically stable α-crystal form by increasing the gap size. The polymer chains were thought to be oriented perpendicular to the fiber direction, and the molecular orientation to the fiber axis was enhanced on increasing the gap size. Addition of salts into an electrospinning system is often a useful way to control the fiber structures and properties. For instance, Mituppatham et al. [35] added NaCl, LiCl and $MgCl_2$ to solutions of nylon-6 in formic acid and found that increasing the salt concentration increased solution viscosity, conductivity and fiber diameter, suggesting that the increase in fiber diameter was due to an increased solution viscosity. As expected, by mixing the additives in the polymer solution for electrospinning, the polymer solution conductivity as well as the solution viscosity is extensively changed and thereby fiber spinnability as well as the fiber structure and properties can be significantly altered depending on the interactions between salt, polymer and solvent [36-38]. However, to date no report has yet been published concerning the mechanical properties of nylon-6 nanofibers containing additives that could be affected by a change in crystalline structure. The aim

of this study was to fabricate nylon-6/$FeCl_2$ nanofiber mats with different concentrations of Fe^{2+} ion additives via electrospinning, and to report the effects of the Fe^{2+} ion additives on the crystalline structure and mechanical properties of the resulting electrospun nylon-6/$FeCl_2$ nanofibers.

4.2 Experimental

4.2.1 Materials

Nylon-6 pellets (relative viscosity ca 2.8) were kindly supplied by Kolon Industries (Gwacheon-SI, Republic of Korea).The pellets were vacuum dried at 60 ^{o}C before use. Formic acid (88%; contains 12% water as stabilizer) and $FeCl_2 \cdot 4H_2O$ (iron(II) chloride tetrahydrate) were purchased from Wako Pure Chemical Industries Ltd (Japan). All these reagents were used without further purification.

4.2.2 Electrospinning

The electrospinning experiments were performed at room temperature, and the apparatus for electrospinning was assembled on the basis of our previous study [2, 11-13]. All polymer solutions prepared were poured in a 5-mL plastic syringe attached to a capillary needle with an inner diameter of 0.6 mm. A copper wire connected to the anode was inserted into the solution, and the cathode was attached to a grounded rotating metallic collector wrapped in aluminum foil. Electrospinning was carried out using the above solutions, with an applied voltage of 13 kV and a tip to collector distance of 15 cm. The electric field was produced by a high voltage power supply (HAR-100*12, Matsusada Co., Japan) capable of generating voltages up to 100 kV. The nylon-6/$FeCl_2$ solutions used for electrospinning were produced as follows. First, 22 wt% nylon-6 solutions were made in formic acid [34]. Next, $FeCl_2 \cdot 4H_2O$ additives with different weight percentages (ϕFe) ranging from 0 to 20 wt% were added into the nylon-6

solutions to produce nylon-6/$FeCl_2$ solutions.

4.2.3 Characterization

Solution properties, such as viscosity and electrical conductivity, were measured with a rheometer (DV-I Prime, Brookfield Co., USA) and a conductance meter (ES-51, Horiba Ltd, Japan), respectively. The morphologies of electrospun nylon-6/$FeCl_2$ nanofibers were examined by SEM (VE-8800, Keyence Co., Japan). The bonding configurations of the electrospun nanofibers were characterized by means of Fourier transform infrared (FTIR) spectroscopy (IR Prestige-21, Shimadzu Co., Japan). The spectra were recorded from 400 to 4000 cm^{-1} with a resolution of 4 cm^{-1} and the addition of 128 scans. The crystal structure of the nylon-6/$FeCl_2$ nanofibers was characterized by wide angle X-ray diffraction (WAXD) (X-ray diffractometer, Rigaku Co., Japan) operating at 40 kV and 150 mA using Cu Kα radiation. Scans were recorded over the 2θ range 15-30 ^{o}. The thermal stability of the nylon-6/$FeCl_2$ nanofibers was investigated by DSC (Thermo plus DSC8230, Rigaku Co., Japan) by heating from 50 to 250 ^{o}C under a continuous nitrogen purge of 10 mL min^{-1}; the heating rate was 10 ^{o}C min^{-1}.

4.2.4 Mechanical properties

Nylon-6/FeCl2 nanofiber mats

The mechanical behaviors of nylon-6/$FeCl_2$ nanofiber mats were determined with a universal testing machine (Tensilon RTC1250A, A&D Co. Ltd, Japan) at a

crosshead speed of 10 mm min^{-1} at room temperature. In accordance with ASTM D-638, samples were prepared in the form of a dumbbell shape and then at least five specimens were tested for tensile behavior and the averaged values are reported. Three parameters were determined from each stress-strain curve: Young's modulus, tensile strength and elongation at break. Tensile strength was calculated using

$$\text{Tensile strength (MPa)} = F/A \qquad (1)$$

where F is the maximum load of force at failure and A is the cross sectional area of the nanofiber specimen. The strain corresponding to the tensile strength is the failure strain. Elongation was calculated as

$$\text{Elongation (\%)} = [(L - L_0)/L_0] \times 100 \qquad (2)$$

where L_0 refers to the initial length of the sample and L is the final length at the break point. The elastic modulus or Young's modulus was calculated from the initial slope of the straight line of the stress-strain curve in the elastic region.

Nylon-6/FeCl2 single nanofibers

Furthermore, the mechanical properties of electrospun nylon-6/$FeCl_2$ single nanofibers were evaluated by the tensile tester developed for single nanofibers (Fitron NFR-1000, RHESCA Co., Japan), as seen in Fig. 1(a). The tester basically consisted of an electronic load sensor for tensile force measurement, Z position stage, fiber holding units, a liquid container and a personal computer for controlling the system operation. The sample frame for collecting a single nanofiber is shown in Fig. 1(b) (top). We collected several oriented nanofibers on a sample holder, as shown in Fig. 1(b) (bottom). Except for a well-aligned nanofiber, other nanofibers which are not well aligned to the

stress axis were eliminated using an optical microscope (High-Resolution Zoom Lens, VH-Z500R Keyence Co., Japan; ×500 to ×5000 zoom range, numerical aperture ca 0.82 at a distance of 0.17 in Fig. 1(b), top). After one fiber is selected and pasted with adhesive on the sample holder, the fiber axis is precisely set to align the stress axis of the holder using optical microscopy. For the fiber diameters, five different points on a single nanofiber were measured to obtain the fiber diameter before the tensile test, and the averaged values were used to convert the force to stress. It should be noted that it took several attempts to get a single nanofiber well aligned to the stress axis, which is indeed a time-consuming process. The main specifications of the system are as follows: maximum loading capacity 500 mN, stroke 20 mm, loading speed 5-20 μm s^{-1}, displacement sensitivity 1.0 μm, loading sensitivity 1.0 μN etc. Three parameters were determined from each stress-strain curve: Young's modulus, tensile strength and elongation at break. The tensile test of single nanofibers was performed at least five times for nanofibers fabricated with several different amounts of Fe^{2+} ion additive.

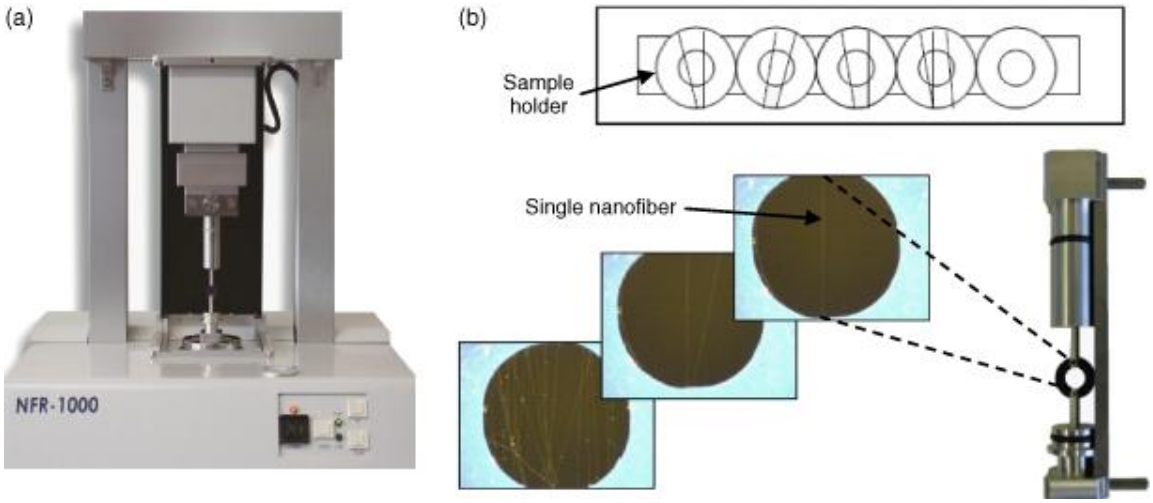

Figure 1 Apparatus for the single nanofiber tensile tester (a) and setup for the uniaxial tensile test of a single nanofiber (b).

4.3 Results and discussion

4.3.1 Morphologies of the electrospun nylon-6/$FeCl_2$ nanofibers

It is well known that electrospun nanofibers are remarkably affected by solution parameters (viscosity, polymer concentration, molecular weight and its distribution in the polymer, electrical conductivity and surface tension), processing parameters (applied voltage, distance from needle to collector, feeding ratio of polymer solution and needle diameter) and ambient parameters (temperature, humidity and atmospheric pressure) during the electrospinning process [11-13]. First, in this work various contents of $FeCl_2 \cdot 4H_2O$ additive were investigated to find the optimum spinning condition of nylon-6/$FeCl_2$ composite solutions on electrospinning. Figures 2(a)-(e) show SEM images of nylon-6/$FeCl_2$ nanofibers electrospun from a solution with various additive contents (ϕFe). From these images it is clear that the pristine nylon-6 nanofiber mat does not form a spider's-web-like morphology, whereas the nylon-6 nanofiber mat with ϕFe ~ 10 wt% exhibits a partly interconnected spider's-web-like morphology [39-41] (Fig. 2(b)). Moreover, such spider's-web-like morphologies became evident with increasing ϕFe. The formation of a spider's-web-like structure may be due to the increased ionization of the polymer solution in the presence of $FeCl_2 \cdot 4H_2O$ additive during electrospinning. A plausible mechanism can be proposed [31]. That is, formic acid, a polar monoprotic solvent with high dielectric constant, is capable of attacking the lactam of nylon-6 to produce a series of short chain oligomer/monomer ions ($-CONH_2^+-$) [42]. The C=O and N-H portion of the ionic species of nylon-6 can hold $FeCl_2 \cdot 4H_2O$ aggregates on the surface of the nanofibers. These ionic polymeric species and $FeCl_2 \cdot$

$4H_2O$ aggregates are connected either by hydrogen bonding or by the formation of complexes with polymer ligands caused by the lone pair of electrons of nitrogen and oxygen, which eventually result in spider's-web-like morphologies. Furthermore, at higher ϕFe (≥15 wt%), very fine nanofibers with diameters of about 30 nm were conspicuous. Such high aspect ratio nanofibers were strongly bound between the main fibers. In general, salts have often been utilized to improve the physicochemical properties of electrospun polymer nanofiber mats by modification of the internal structure. For instance, Ding et al. [39] observed a fishnet-like morphology in electrospun nylon-6 and poly (acrylic acid) (PAA) nanofibers. Nylon-6, polyurethane and poly(vinyl alcohol) polymeric nanofiber mats containing a spider's-web morphology have been synthesized by the addition of metallic salt. [40] Parajuli et al. [41] reported a spider's-web-like arrangement of fibers with an average diameter of 18 nm by the polymerization of PAA with nylon. The growing interest in the utilization of these nanostructures primarily stems from the unique physical, mechanical and electrical properties associated with their very high surface areas. These properties make nanofibers suitable for the creation of numerous technologically advanced products within many fields of application. In addition, the average diameters of electrospun nylon-6/$FeCl_2$ nanofibers gradually increased with increasing ϕFe, presumably due to increased solution viscosity via a gradual increase in ionic crosslinking density in terms of the added Fe^{2+} ions. The fiber diameters, viscosities and electrical conductivities of electrospun nylon-6/$FeCl_2$ nanofiber mats with different ϕFe are shown in Fig. 3.

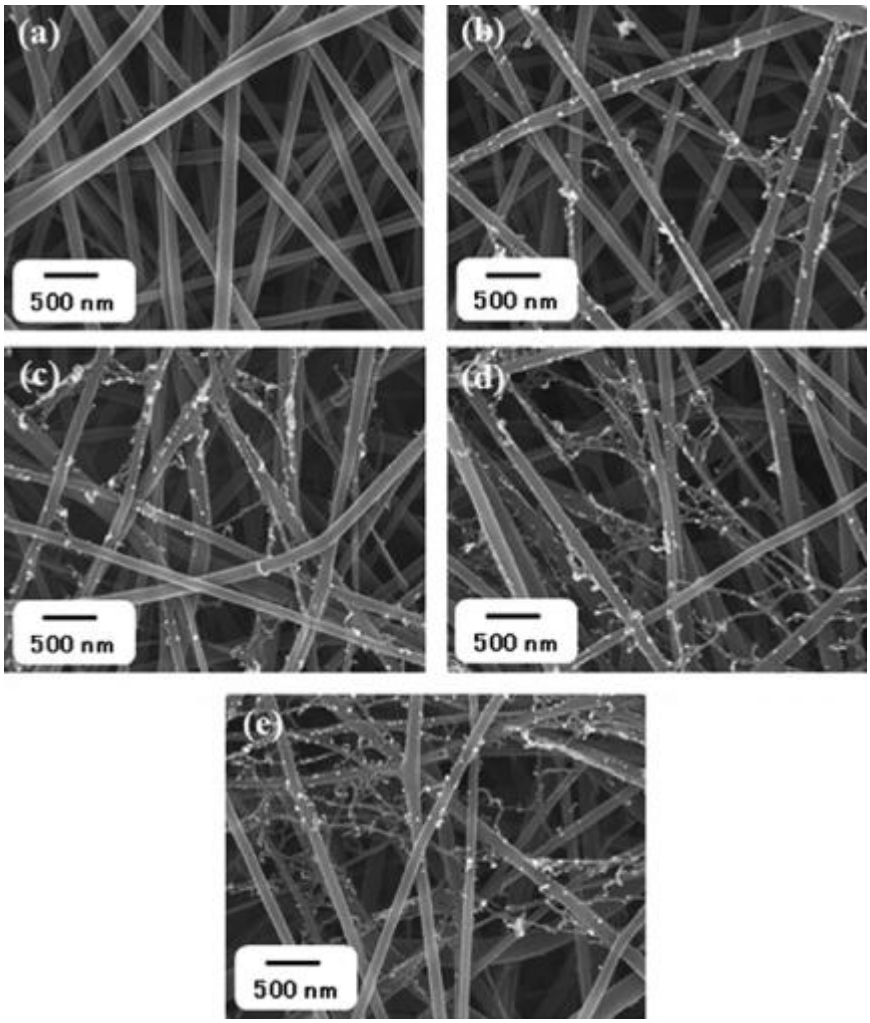

Figure 2 SEM images of electrospun nylon-6/$FeCl_2$ nanofibers fabricated with various ϕFe: (a) 0, (b) 5, (c) 10, (d) 15 and (e) 20 wt%.

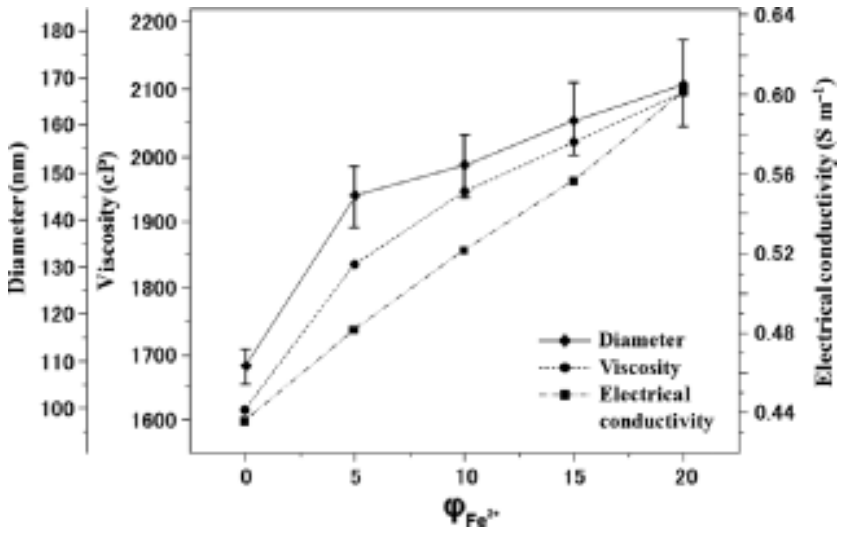

Figure 3 Viscosity, electrical conductivity and average fiber diameter of nylon-6/$FeCl_2$ solutions with various ϕFe. All nylon-6 solution concentrations were 22 wt%.

4.3.2 FTIR analysis

FTIR spectroscopy was used to investigate the changes in the bonding configurations and secondary molecular interactions in electrospun nylon-6/$FeCl_2$ nanofibers. Figure 4 shows FTIR spectra of the electrospun nylon-6/$FeCl_2$ nanofibers with different ϕFe. The characteristic bands at 1540.0 and 1560.4 cm^{-1} correspond to amide II (mainly attributed to C-N stretching and N-H bending, respectively). The band at 1647.2 cm^{-1} corresponds to amide I (attributed to the C=O band). It was clearly observed that the absorption peaks of amide I (ca 1650 cm^{-1}) and amide II (ca 1550 cm^{-1}) were greatly changed, indicating a change in molecular interactions and crystalline structures. That is, the peak band at 1560.4 cm^{-1} increased and gradually became sharper with increasing ϕFe. Moreover, the peak band at 1647.2 cm^{-1} is slightly red shifted to 1643.0 cm^{-1}, while the peak band at 1540.0 cm^{-1} is blue shifted to 1543.0 cm^{-1}. The results also coincide well with a previous report [43] that the complex formation of salts ($GaCl_3$) with the C=O groups in nylon-6 chains causes the N-H vibrational band to shift to a higher frequency (red shift), while the C=O vibrational band shifts to lower frequency (blue shift) due to a reduction in bond order as a result of complexation. In addition, a further increase of additives (ions) starts to initiate a polyelectrolytic nature of nylon-6 dissolved in formic acid, due to the partial ionization of the amide groups along the polymer backbone, and therefore results in splitting up of very fine nanofibers from the main nanofibers during electrospinning. (For example, Fe^{2+} free ions form a complex with C=O groups. At this stage, these highly ionized parts cannot stay between the main nanofibers. Rather, they simply escape from the main nanofibers due to very high ionized states [40].)

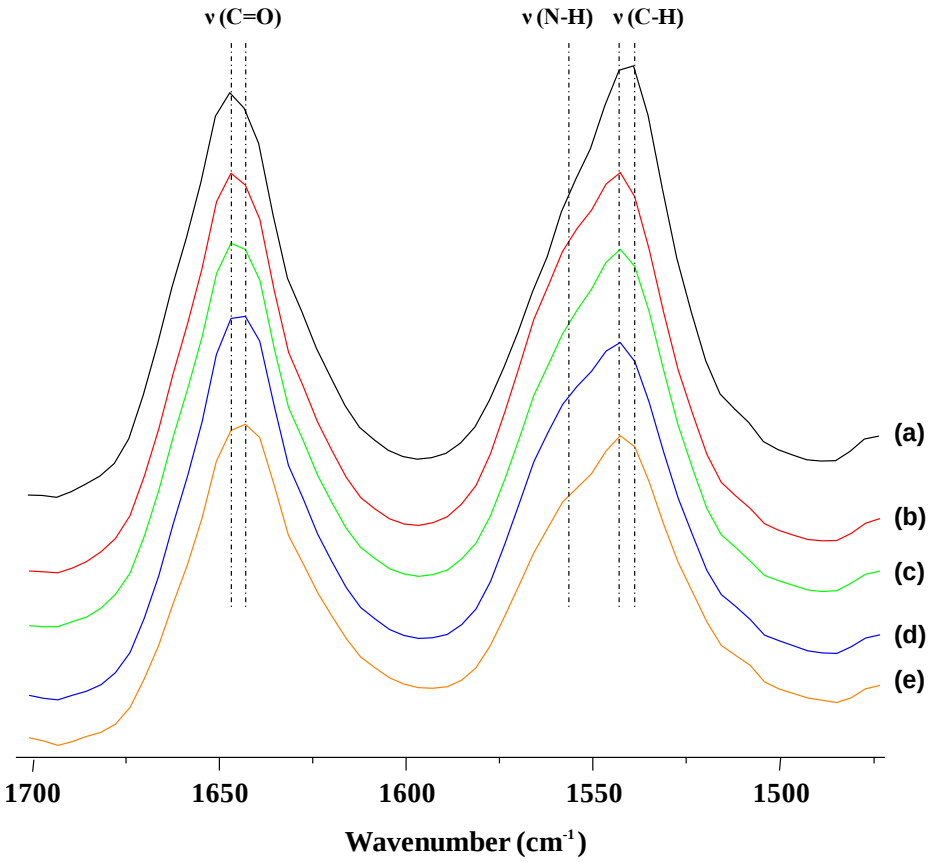

Figure 4 FTIR spectra of the electrospun nylon-6/$FeCl_2$ nanofibers with various ϕFe: (a) 0 wt%, (b) 5 wt%, (c) 10 wt%, (d) 15 wt%, and (e) 20 wt%. All nylon-6 solution concentrations were 22 wt%.

4.3.3 WAXD analysis

In general, it is known that the α-form exhibits two characteristic reflections at $2\theta = 20.3^{o}$ and $2\theta = 23.7^{o}$, whereas the γ-form exhibits a characteristic reflection at $2\theta = 21.3^{o}$. In this work, the effects of Fe^{2+} ions on the crystalline structure of the resulting electrospun nylon-6/$FeCl_2$ nanofibers were investigated. Figure 5 shows WA XD patterns of electrospun nylon-6/$FeCl_2$ nanofibers with different ϕFe. The electrospun pure nylon-6 nanofibers clearly present typical diffraction peaks at $2\theta = 21.4^{o}$, characteristic of the γ-form (d spacing 0.42 nm), and at 20.5^{o} and 23.3^{o}, characteristic of the α-form (d spacing 0.433 and 0.381 nm). The result also indicates that the metastable γ-form is predominant in the as spun nylon-6 nanofibers. However, the relative intensity of such γ-form gradually decreases with increasing ϕFe, indicative of the transformation of the crystalline structure in the electrospun nylon-6/$FeCl_2$ nanofibers due to strong molecular interactions between the nylon-6 backbone and the additive Fe^{2+} ions. In particular, at higher ϕFe (≥15 wt%) the intensity of the γ-form was drastically decreased and the intensity of the α-form became evident. This result is significant and also coincided well with the FTIR analysis.

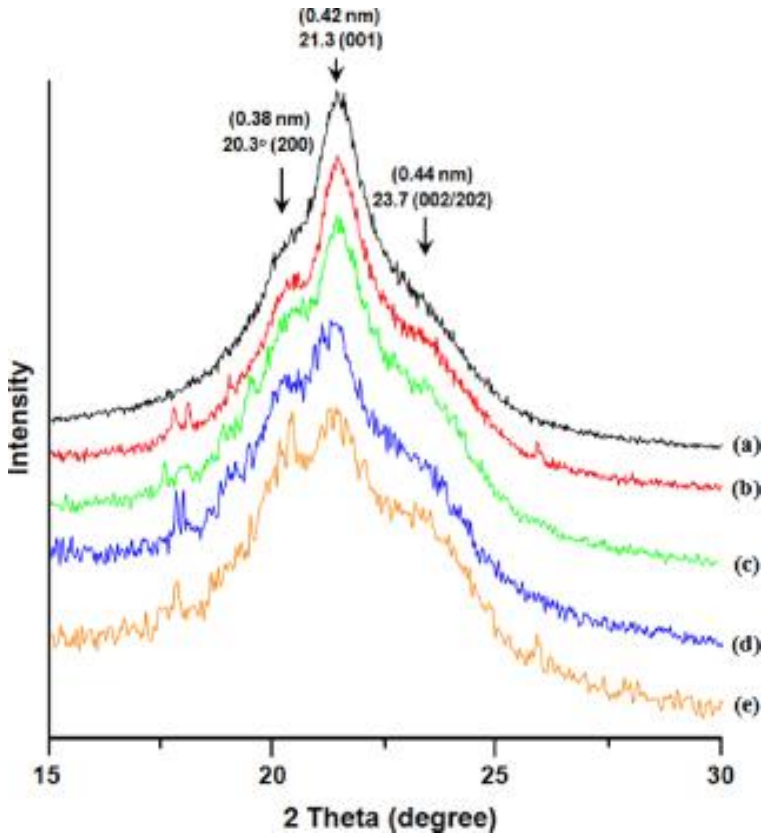

Figure 5 WAXD patterns of electrospun nylon-6/$FeCl_2$ nanofibers with various ϕFe: (a) 0 wt%, (b) 5 wt%, (c) 10 wt%, (d) 15 wt%, and (e) 20 wt%.

4.3.4 Thermal analysis

The crystallization behavior of electrospun nylon-6/$FeCl_2$ nanofibers was also investigated using DSC. Figure 6 shows that DSC thermograms (second scans) of the electrospun nylon-6/$FeCl_2$ nanofibers with different ϕFe. The electrospun pure nylon-6 nanofibers exhibited melting temperatures at 223.9 and 214.0 ^oC corresponding to α-form crystals (◆) and γ-form crystals (●), respectively [44]. The gradual decrease in the melting points of α- and γ-form crystals with an increase of ϕFe indicates that incorporation of additive Fe^{2+} ions onto nylon-6 nanofibers hinders the crystallization process and results in crystallites with lower thermal stability. Moreover, it was also found that the electrospun nylon-6/$FeCl_2$ nanofibers with ϕFe = 20 wt% did not show sharp endothermic peaks. Additionally, the degree of crystallinity of the electrospun nylon-6/$FeCl_2$ nanofibers can be estimated by integrating the melt endotherm (heat of fusion, ΔH_f) and calculating the ratio with that (ΔH_f^0) of a theoretical 100% crystalline nylon-6. In this study, a ΔH_f^0 value [44] of 240 J/g was used to calculate the degree of crystallinity of the electrospun nylon-6 nanofibers. The calculated crystallinity values of the electrospun nylon-6/$FeCl_2$ nanofibers with ϕFe of 0, 5, 10, 15 and 20 wt% were found to be 29.5%, 26.2%, 22.2%, 19.5% and 16.6%, respectively. The results indicate that the crystalline structure of electrospun nylon-6/$FeCl_2$ nanofibers was destroyed as a function of the amount of additives, which was also coincided well with the FTIR and WAXD analysis data.

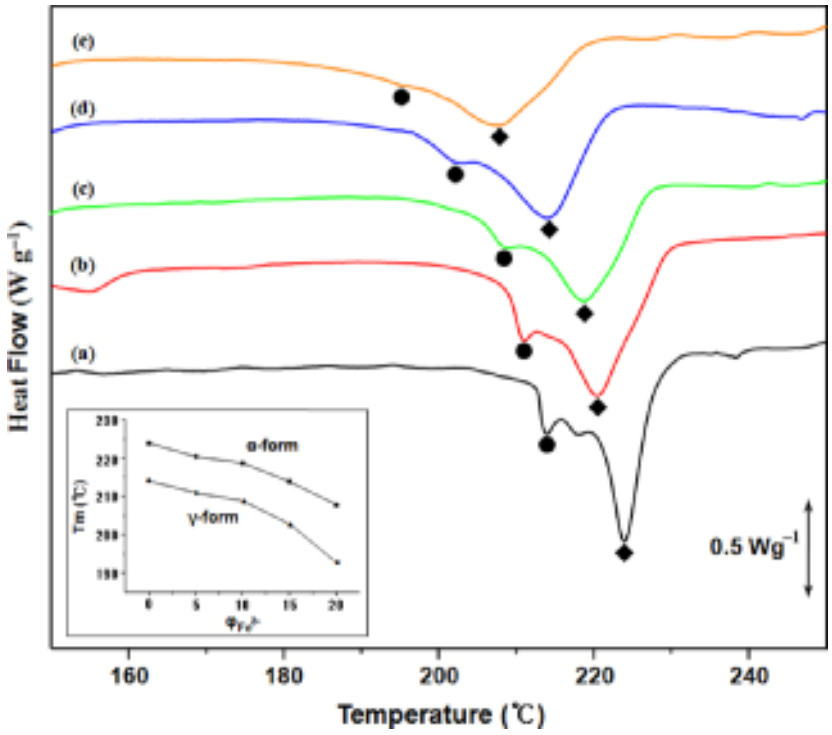

Figure 6 DSC heating scans of electrospun nylon-6/FeCl2 nanofibers with various ϕFe: (a) 0 wt%, (b) 5 wt%, (c) 10 wt%, (d) 15 wt%, and (e) 20 wt%. The symbols show the melting point of two crystalline structures, α-form (◆) and γ-form (●).

4.3.5 Mechanical properties

Nylon-6/$FeCl_2$ nanofiber mats

Figure 7 shows typical stress–strain curves of the electrospun nylon-6/$FeCl_2$ nanofiber mats with different ϕFe, showing a peculiar characteristic of the elastomers. In comparison with electrospun pure nylon-6 nanofiber mats (tensile strength ca 11.1 MPa), all electrospun nylon-6/$FeCl_2$ nanofiber mats showed lower tensile strength values (ranging from about 9.7 to 10.3 MPa, depending on the amount of Fe^{2+} additive). The elongation at break decreased slightly with increasing ϕFe. In contrast, Young's modulus increased gradually with increasing ϕFe. That is, Young's modulus of electrospun pure nylon-6 nanofiber mats was about 156.5 MPa, whereas the electrospun nylon-6/$FeCl_2$ mats with ϕFe ~ 20 wt% exhibited a Young's modulus about 1.5 times higher (ca 239.6 MPa). Although this is not fully understood, it could be attributed to the unique nanofiber morphology, such as the spider's-web-like morphology, contributing to the increase in modulus as a linker between the fibers at an initial stretching stage (within the elastic region). This should be further studied in detail and will be reported later. Indeed, as seen in SEM images of electrospun nylon- 6/$FeCl_2$ nanofiber mats, many very fine nanofibers (ca 30 nm in fiber diameter) were observed and also increased with increasing additive. As a result, such spider's-web-like morphology critically contributed to the increase in Young's modulus of electrospun nylon-6/$FeCl_2$ nanofiber mats.

Nylon-6/$FeCl_2$ single nanofiber

In order to investigate the intrinsic mechanical properties of electrospun nylon-6/$FeCl_2$ nanofibers, stress–strain studies of single electrospun nylon-6/$FeCl_2$ nanofibers with different ϕFe were carried out (Fig. 8). It should be noted that we attempted to collect nanofibers on a sample holder until we got nanofibers without a spider's-web structure, which was important to exactly evaluate the mechanical properties of single nanofiber. As a result, the strain and ultimate stress of an electrospun pure nylon-6 single nanofiber were found to be 67.3% and 320.9 MPa, respectively. Also, an electrospun nylon-6/$FeCl_2$ single nanofiber with ϕFe =5 wt% exhibited a slightly higher tensile strength (391.1 MPa), indicating that the nylon-6/$FeCl_2$ single nanofiber became stiffer and stronger. These results might be due to crosslinking and stiffening by incorporating the additive Fe^{2+} ions (a major contribution to the mechanical properties), even though there was a slight decrease in crystallinity (minor contribution to the mechanical properties). On the other hand, when ϕFe was further increased to 20 wt%, the strain drastically decreased to 8.1% but the stress slightly decreased to 358.8 MPa. Also, Young's modulus exponentially increased from about 1.46 to 5.26 GPa with increasing ϕFe. It was therefore considered that Young's modulus significantly increased with increasing ϕFe. The detailed values of each tensile test are summarized in Table 1.

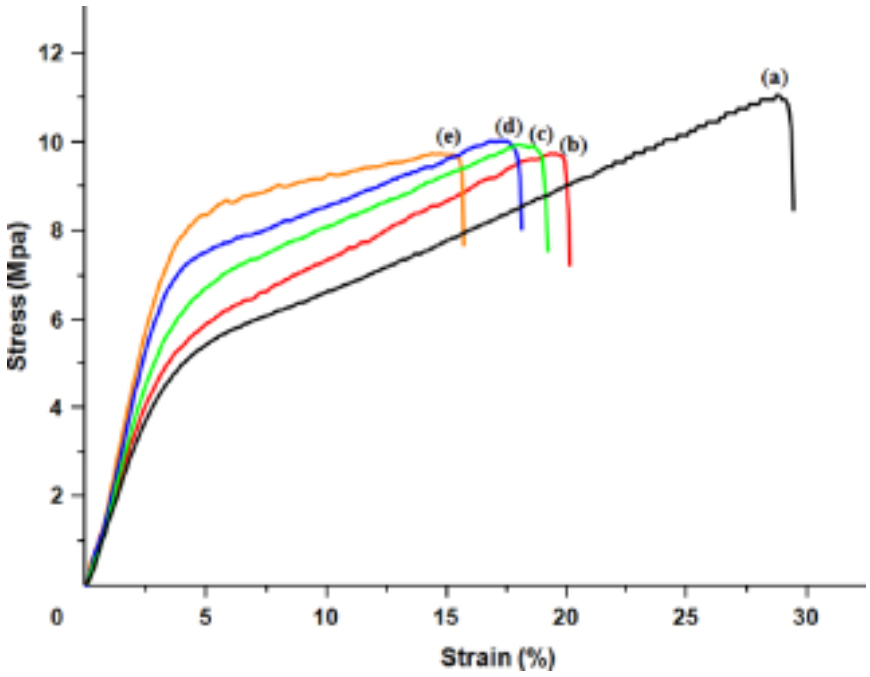

Figure 7 Tensile strength of electrospun nylon-6/$FeCl_2$ nanofibers with various ϕFe: (a) 0 wt%, (b) 5 wt%, (c) 10 wt%, (d) 15 wt%, and (e) 20 wt%.

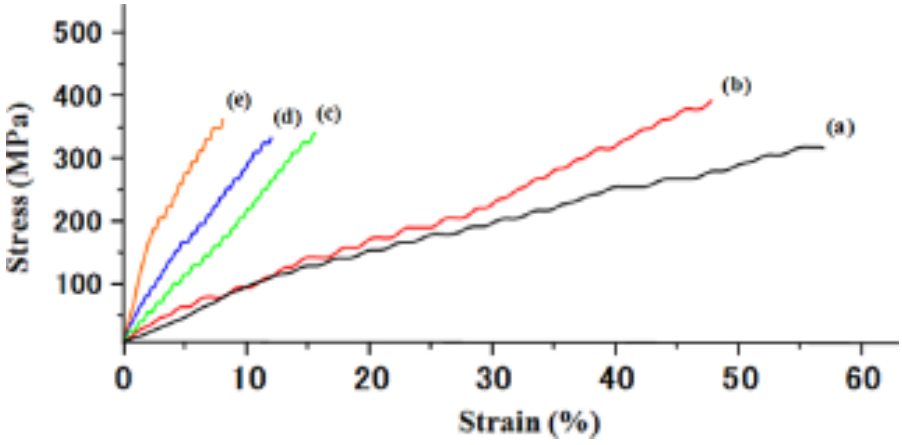

Figure 8 Tensile strength of electrospun nylon-6/FeCl2 single nanofibers with various ϕFe: (a) 0 wt%, (b) 5 wt%, (c) 10 wt%, (d) 15 wt%, and (e) 20 wt%.

Table 1 Detailed value of Young's modulus, tensile strength and elongation at break point

Hybrid nanofibers	φ_{Fe}	Young's modulus (MPa)	Tensile strength (MPa)	Elongation at break (%)
Nonwoven nylon-6/$FeCl_2$ nanofiber mats	0	156.5	11.1	28.8
	5	168.2	9.7	19.9
	10	183.8	9.9	18.8
	15	202.4	10.5	17.5
	20	239.6	9.8	15.3
Single nylon-6/$FeCl_2$ nanofiber	0	1460	320.9	67.3
	5	1818	391.1	47.9
	10	3137	345.2	15.8
	15	4054	330.5	12.6
	20	5260	358.8	8.1

4.4 References

[1] K. Zhang, L.L. Zhao, J. Wu, Graphene/Polyaniline Nanofiber Composites as Supercapacitor Electrodes, Chem. Mater. 22 (2010) 1392-1401.

[2] J. Venugopal, S. Low, A. T. Choon, S. Ramakrishna, Interaction of Cells and Nanofiber Scaffolds in Tissue Engineering, J. Biomed. Mater. Res. B Appl. Biomater. 84B (2008) 34-48.

[3] B.S. Kim, I.S. Kim, Recent Nanofiber Technologies: A Perspective for a Special Issue of Polymer Reviews, Polym. Rev. 51 (2011) 235-238.

[4] A. Suzuki, Y. Yamada, Poly(ethylene-2,6-naphthalate) Nanofiber Prepared by Carbon Dioxide Laser Supersonic Drawing, J. Appl. Polym. Sci. 116 (2010) 1913-1919.

[5] G. Che, B.B. Lakshmi, E.R. Fisher, C.R. Martin, Carbon nanotubule membranes for electrochemical energy storage and production, Nature 393 (1998) 346-349.

[6] S.L. Tao, T.A. Desai, Aligned Arrays of Biodegradable Poly(*å*-caprolactone) Nanowires and Nanofibers by Template Synthesis, Nano Lett. 7 (2007) 1463-1468.

[7] S.E.Paramonov, H.-W. Jun, J.D. Hartgerink, Self-Assembly of Peptide-Amphiphile Nanofibers: The Roles of Hydrogen Bonding and Amphiphilic Packing, J. Am. Chem. Soc. 128 (2006) 7291-7298.

[8] W. Zhang, S.S. Liao, F.Z. Cui, Hierarchical Self Assembly of Nano-Fibrils in Mineralized Collagen, Chem. Mater. 15 (2003) 3221-3226.

[9] S.-H. Yu, M. Antonietti, H. Colfen, J. Hartmann, Growth and Self-Assembly of $BaCrO_4$ and $BaSO_4$ Nanofibers toward Hierarchical and Repetitive

Superstructures by Polymer-Controlled Mineralization Reactions, Nano Lett. 3 (2003) 379-382.

[10] L. He, Y. Zhang, X. Zeng, D. Quan, S. Liao, Y. Zeng, J. Lu, S. Ramakrishna, Fabrication and characterization of poly(L-lactic acid) 3D nanofibrous scaffolds with controlled architecture by liquid−liquid phase separation from a ternary polymer−solvent system, Polym. 50 (2009) 4128-4138.

[11] O. Ohsawa, K.-H. Lee, B.-S. Kim, S. Lee, I.-S. Kim, Preparation and characterization of polyketone (PK) fibrous membrane via electrospinning, Polym. 51 (2010) 2007-2012.

[12] K. Watanabe, B.S. Kim, I.S. Kim, Development of Polypropylene Nanofiber Production System, Polym. Rev. 51 (2011) 288-308.

[13] Y.J. Lee, J. Lee, D. Kimura, B. S. Kim, J. Koh, I.S. Kim, Effects ofmechanical force on crystalline structure of electrospun poly(1-butene) membranes, Polym. Int. 60 (2011) 1442-1445.

[14] W. Sambaer, M. Zatloukal, D. Kimmer, 3D modeling of filtration process via polyurethane nanofiber based nonwoven filters prepared by electrospinning process, Chem. Eng. Sci. 66 (2011) 613-623.

[15] S. Lin, Q. Cai, J. Ji, G. Sui, Y. Yu, X. Yang, Q. Ma, Y. Wei, X. Deng, Electrospun nanofiber reinforced and toughened composites through in situ nano-interface formation, Compos. Sci. Technol. 68 (2008) 3322-3329.

[16] L. Shao, W. Ji, P. Dong, M. Zeng, C. Qi, X.M. Zhang, Coupling reactions of aromatic halides with palladium catalyst immobilized on poly(vinyl alcohol) nanofiber mats, Appl. Catal. A 413-4 (2012) 267-272.

[17] J. Moon, J.A. Park, S.J. Lee, T. Zyung, I.D. Kim, Pd-doped TiO2 nanofiber

networks for gas sensor applications, Sens. Actuators B 149 (2010) 301-305.

[18] R. Uppal, G.N. Ramaswamy, C. Arnold, R. Goodband, Y. Wang, Hyaluronic acid nanofiber wound dressing–production, characterization, and in vivo behavior, J. Biomed. Mater. Res. B Appl. Biomater. 97B (2011) 20-29.

[19] S.Y. Hyuk, T.G. Kim, T.G. Park, Surface-functionalized electrospun nanofibers for tissue engineering and drug delivery, Adv. Drug Deliv. Rev. 61 (2009) 1033-1042.

[20] K. Wei, Y. Li, K.O. Kim, Y. Nakagawa, B.S. Kim, K. Abe, G.Q. Chen, I.S. Kim, Fabrication of nano-hydroxyapatite on electrospun silk fibroin nanofiber and their effects in osteoblastic behavior, J. Biomed. Mater. Res. A 97A (2011) 272-280.

[21] K. Song, J.F. Rabolt, Polarized Raman Measurements of Uniaxially Oriented Poly (ε-caprolactam), Macromol. 34 (2001) 1650-1654.

[22] D.R. Holmes, C.W. Bunn, D.J. Smith, The crystal structure of polycaproamide: Nylon 6, J. Polym. Sci. 17 (1955) 159-177.

[23] A. Okada, M. Kawasumi, I. Tajima, T. Kurauchi, O. Kamigaito, A solid state NMR study on crystalline forms of nylon 6 , J. Appl. Polym. Sci. 37 (1989) 1363-1371.

[24] R. Dersch, T. Liu, A.K. Schaper, A. Greiner, J.H. Wendorff, Electrospun Nanofibers: Internal Structure and Intrinsic Orientation, J. Polym. Sci. 41 (2003) 545-553.

[25] J. A. Matthews, G.E. Wnek, D.G. Simpson, G.L. Bowlin, Electrospinning of Collagen Nanofibers, Biomacromol. 3 (2002) 232-238.

[26] W.E. Teo, M. Kotaki, X.M. Mo, S. Ramakrishna, Porous tubular structures with

controlled fibre orientation using a modified electrospinning method, Nanotechnol. 16 (2005) 918-924.

[27] J.H. Park, B.S. Kim, Y.C. Yoo, M.S. Khil, H.Y. Kim, Enhanced Mechanical Properties of Multilayer Nano-Coated Electrospun Nylon 6 Fibers via a Layer-by-Layer Self-Assembly, J. Appl. Polym. Sci. 107 (2008) 2211-2216.

[28] Y. Liu, F. Guan, Y. Gao, N.E. Hedin, L. Zhu, H. Fong, Crystalline Morphology and Polymorphic Phase Transitions in Electrospun Nylon-6 Nanofibers, Macromol. 40 (2007) 6283-6290.

[29] T. Ishisue, M. Okamoto, K. Tashiro, Real-time investigation of crystallization in nylon 6-clay nano-composite probed by infrared spectroscopy, Polym. 51 (2010) 5585-5591.

[30] M.V. Jose, B.W. Steinert, V. Thomas, D.R. Dean, M.A. Abdalla, G. Price, G.M. Janowski, Morphology and mechanical properties of Nylon 6/MWNT nanofibers, Polym. 48 (2007) 1096-1104.

[31] H.R. Pant, M.P. Bajgai, K.T. Nam, Y.A. Seo, D.R. Pandeya, S.T. Hong, H.Y. Kim, Electrospun nylon-6 spider-net like nanofiber mat containing TiO_2 nanoparticles: A multifunctional nanocomposite textile material, J. Hazard. Mater. 185 (2011) 124-130.

[32] C. Ibanes, M. de Bpossoeu, L. David, R. Seguela, High temperature behaviour of the crystalline phases in unfilled and clay-filled nylon 6 fibers, Polym. 47 (2006) 5071-5079.

[33] S.-Y. Park, Y.-H.- Cho, R.A. Vaia, Three-Dimensional Structure of the Zone-Drawn Film of the Nylon-6/Layered Silicate Nanocomposites, Macromol. 38 (2005) 1729-1735.

[34] N. Kimura, H.-K. Kim, B.-S. Kim, K.-H. Lee, I.-S. Kim, Molecular Orientation and Crystalline Structure of Aligned Electrospun Nylon-6 Nanofibers: Effect of Gap Size, Macromol. Mater. Eng. 295 (2010) 1090-1096.

[35] C. Mit-uppatham, M. Nithitanakul, P. Supaphol, Ultrafine Electrospun Polyamide-6 Fibers: Effect of Solution Conditions on Morphology and Average Fiber Diameter, Macromol. Chem. Phys. 205 (2004) 2327-2338.

[36] P. Bajaj, S.H. Bahrami, K. Sen, T.V. Sreekumar, Thermal and Rheological Behavior of Acrylonitrile–Carboxylic Acid Copolymers and Their Metal Salt Complexes, J. Appl. Polym. Sci. 74 (1999) 567-582.

[37] Y.W. Cho, S.W. An, S.-C. Song, Effect of Inorganic and Organic Salts on the Thermogelling Behavior of Poly(organophosphazenes), Macromol. Chem. Phus. 207 (2006) 412-418.

[38] M.A. Phadke, D.A. Musale, S.S. Kulkarni, S.K. Karode, Poly(acrylonitrile) Ultrafiltration Membranes. I. Polymer-Salt-Solvent Interactions, J. Polym. Sci. Polym. Phys 43 (2005) 2061-2073.

[39] B. Ding, C. Li, Y. Miyauchi, O. Kuwaki, S. Shiratori, Formation of novel 2D polymer nanowebs via electrospinning, Nanotechnol. 17 (2006) 3685-3691.

[40] N.A.M. Barakat, M.A. Kanjwal, F.A. Sheikh, H.Y. Kim, Spider-net within the N6, PVA and PU electrospun nanofiber mats using salt addition: Novel strategy in the electrospinning process, Polym. 50 (2009) 4389-4396.

[41] D.C. Parajuli, M.P. Bajgai, J.A. Ko, H.K. Kang, M.S. Khil, H.Y. Kim, Synchronized Polymerization and Fabrication of Poly(acrylic acid) and Nylon Hybrid Mats in Electrospinning, Appl. Mater. Interf. 1 (2009) 709-715.

[42] J.R. Schaefgen, C.F. Trivisonno, Polyelectrolyte Behavior of Polyamides. I.

Viscosities of Solutions of Linear Polyamides *in* Formic Acid and *in* Sulfuric Acid, J. Am. Chem. Soc. 73 (1951) 4580-4585.

[43] A. Gupta, C.D. Saquing, M. Afshari, A.E. Tonelli, S.A. Khan, R. Kotek, Porous Nylon-6 Fibers via a Novel Salt-Induced Electrospinning Method, Macromol. 42 (2009) 709-715.

[44] L. Li, L.M. Bellan, H.G. Craighead, M.W. Frey, Formation and properties of nylon-6 and nylon-6/montmorillonite composite nanofibers, Polym. 47 (2006) 6208-6217.

Chapter 5

Fabrication and Characterization of Reinforced Electrospun poly (vinylidenne fluoride-co-hexafluoropropylene) nanofiber membranes

Chapter 5

Fabrication and characterization of reinforced electrospun poly (vinylidene fluoride-co-hexafluoropropylene) nanofiber membranes

Abstract

In this study, poly (vinylidene fluoride-co-hexafluoropropylene) (PVDF-HFP) nanofiber membranes with different amounts of polyethylene glycol (PEG) and polyethylene glycol dimethacrylate (PEGDMA) oligomer were fabricated via electrospinning. The obtained nanofiber membranes were subsequently thermal treated to produce physically bonded structures and chemically cross-linked networks, which were confirmed by scanning electron microscopy (SEM), Fourier transform infrared spectra (FT-IR) and wide-angle x-ray diffraction (WAXD). Young's modulus of electrospun nanofiber membrane with the composition of PVDF-HFP/PEG/PEGDMA (6/1/3, w/w/w) was approximately three times for the case of nanofiber membrane and four times for the case of single nanofiber higher than that of pure PVDF-HFP nanofiber, respectively. The characteristic of cell cycling performance was demonstrated as the possibility of its application at ambient temperature. The electrospun PVDF-HFP nanofiber membrane presented great electrolyte uptake because the membrane had higher porosity due to the structural features of nonwoven fabric, and the amorphous regions in PVDF-HFP could trap large amounts of liquid electrolyte. Also, the cell performance of the membrane as the separator declared high discharge capacity. As the result, the reinforced electrospun

composite nanofiber membrane was found to be a promising candidate as a separator for lithium-ion batteries.

5.1 Introduction

Nanotechnologies, especially nanofibers, have received large numbers of attentions from various fields, such as medicine [1], electrical science [2], and energy resources [3]. As is well known, one of the effective methods of nanofiber fabrication is electrospinning, which has many advantages compared with other conventional methods, such as capability of successive spinning, relative ease, and straightforward method of fabricating nanofibers. So far, some researchers have already attempted to fabricate electrospun nanofibers for the purpose of electrical applications [4, 5]. Cheng et al. [6] developed chemically cross-linked polymer electrolytes via heat-treatment of poly(vinylidene fluoride-co-hexafluoropropylene) (PVDF-HFP) and polyethylene glycol dimethacrylate (PEGDMA) blends. PVDF-HFP has both of crystalline and semi-crystalline (amorphous) regions, chemically high resistance, and relatively high dielectric constant. The amorphous region is capable of trapping large amounts of liquid electrolyte, whereas crystalline region acts to maintain the mechanical properties. Cheng et al. [7] also reported the PVDF-HFP based gel electrolytes prepared by a combination of controlled solvent evaporation and thermal polymerization with PEGDMA. This material exhibited both high ambient ionic conductivity as well as high tensile strain by using polyethylene glycol (PEG) as a plasticizer. Based on these former works, it was considered that PVDF-HFP copolymer was a suitable material for producing separators. PEGDMA and PEG played an important role of improving the mechanical strength and tensile strain.

Recently, rapid growing demands for rechargeable lithium-ion batteries (LIBs) [8, 9] have motivated a lot of researchers to develop new separator materials. A separator

is necessary to divide positive and negative electrode and retain liquid electrolyte. Also, it has to have many fine pores because lithium-ion needs to pass between the electrodes in order to perform charge-discharge behavior, and this cycling performance should be kept after many cycling behavior. The existing commercial separator has low ionic conductivity because of low electrolyte uptake [10], and resistance property is poor often due to the dendrites arising from charge-discharge cycling [11]. To solve these issues, the development of electrospun nanofiber membrane having high surface area, porosity, and laminated structure, is considered to be very important. However, mechanical properties of electrospun nanofiber membrane as a separator are exceptionally-low [4, 10]. Even if cell performance is improved by using nanofiber membrane as the separator, we cannot use it if the membrane is unendurable during cell assembly. Therefore, we attempted to prepare reinforced electrospun nanofiber membrane.

In this study, the PVDF-HFP/PEG/PEGDMA nanofiber membranes were prepared via electrospinning from the solutions of different blend ratio. Afterwards, these electrospun nanofiber membranes were thermal-treated in order to develop physically bonded structures and chemically cross-linked networks. Characteristics of mechanical behaviors of electrospun nanofiber membrane and single nanofiber were investigated. To our knowledge, the reports on mechanical properties of single nanofibers are few. Also, the characteristic of cell cycling performance at ambient environment were demonstrated for investigating the possibility of the membrane as a separator in LIBs applications.

5.2 Experimental

5.2.1 Preparation of electrospun PVDF-HFP/PEG/PEGDMA nanofiber membranes

The solution for electrospinning was prepared by dissolving poly (vinylidene fluoride-co-hexafluoropropylene) (PVDF-HFP) (average Mw = 400,000 g/mol, Sigma Aldrich, Ltd.) in a mixture of acetone and dimethylacetamide (DMAc) (Wako Pure Chemical Industries, Ltd., Japan) (7/3, w/w) to achieve a polymer concentration of 16 wt%. Then, the solution was mixed with polyethylene glycol (PEG, Mw = 400 g/mol) and polyethylene glycol dimethacrylate (PEGDMA, Mw = 550 g/mol) oligomer (Wako Pure Chemical Industries, Ltd., Japan). The polymer solution was dissolved at room temperature with the help of a magnetic stirrer for 2 h until a homogeneous solution was completed. The PVDF-HFP/PEG/PEGDMA solutions were made by mixing various composition ratio of 6/4/0, 6/3/1, 6/2/2, 6/1/3, and 6/0/4 (w/w/w) [PVDF-HFP/PEG/PEGDMA-640, -631, -622, -613, and -604]. The purified 2, 2'-azobisisobutyronitrile (AIBN) (Wako Pure Chemical Industries, Ltd., Japan) of 2 wt% as an initiator was added to each solution.

The electrospinning experiments were performed at room temperature as our previous reports [12-14]. The solution was loaded in a plastic tube connected with a 20 G capillary tip in which there was a copper wire as an electrode, the collecting roller was placed at a distance of 12 cm from the capillary tip, and a voltage of 11 kV was applied by a high voltage power supply (HAR-100*12, Matsusada. Co., Japan). Finally, each electrospun PVDF-HFP/PEG/PEGDMA nanofiber membrane was thermal-treated in an oven at 90 ^{o}C for 24 h to polymerize PEGDMA oligomer. For convenience, each sample

obtained from various composition ratio of the PVDF-HFP/PEG/PEGDMA was denoted as pure PVDF-HFP, PVDF-HFP-640, PVDF-HFP-631, PVDF-HFP-622, PVDF-HFP-613, and PVDF-HFP-604, respectively.

5.2.2 Characterization

The morphologies of electrospun PVDF-HFP/PEG/PEGDMA nanofibers were examined with scanning electron microscope (SEM, JSM-5300, JEOL Ltd., Japan). And the fiber average diameter of each sample was measured from SEM images by using Image-J software.

The mechanical behaviors of electrospun PVDF-HFP/PEG/PEGDMA nanofiber membranes were determined by using a universal testing machine (TENSILON RTC1250A, A&D Company Ltd., Japan) under a crosshead speed of 10 mm/min at ambient temperature (T=23-25 °C). In accordance with ASTM D-638, samples were prepared in the form of a dumbbell-shape. Besides, the mechanical properties of electrospun PVDF-HFP/PEG/PEGDMA single nanofiber were evaluated by the tensile tester developed for measurement of the strength of single-nanofiber (FITRON NFR-1000, RHESCA Co., Japan). The testing process is shown in Fig. 1. The aligned PVDF-HFP/PEG/PEGDMA nanofibers were collected on metal sample frame (Fig. 1a) during electrospinning [13]. The nanofibers which were crossed over each other were eliminated under microscope. The obtained single nanofibers were thermal treated in an oven at 90 °C for 24 h. After that, a suitable single fiber was selected and fixed on the paper cutting sheet (Fig.1b), and the diameter of this chosen single nanofiber was observed by optical microscope. Then, the paper cutting sheet with chosen single

nanofiber was fixed on the sample holder. The fiber axis was precisely set to align the stress axis of the holder using an optical microscopy and two sides of the sheet were cut carefully after the holder was fixed on the tensile tester (Fig. 1c). The measurement was carried out under a crosshead speed of 1 mm/min at ambient temperature (T = 23-25 °C). Three parameters were determined from each stress–strain curve: Young's modulus, tensile strength, and elongation at break.

The molecular structure of PEGDMA networks in electrospun PVDF-HFP/PEG/PEGDMA nanofiber was characterized by means of Fourier transform infrared spectroscopy (FT-IR, IR Prestige-21, SHIMADZU Co., Japan) in a wave number range of 400-4000 cm^{-1} with a resolution of 4 cm^{-1} and the addition of 128 scans under ambient conditions. Also, the prepared nanofiber membranes were subjected to X-ray diffraction (WAXD, X-ray Diffractometer, Rigaku Co., Japan) operating at 40 kV and 150 mA using Cu Kα radiation, and scan were recorded over 2θ range of 15-25^{o}.

The porosity (*P*) was calculated using the following equation (1) [10] by weighing the PVDF-HFP/PEG/PEGDMA nanofiber membrane with and without 1-butanol:

$$P = \frac{W_{wet} - W_{dry}}{\rho_b V_{dry}} \quad (1)$$

where W_{wet} is the weight of the membrane soaked in 1-butanol (Wako Pure Chemical Industries, Ltd., Japan) for 2 h, and then taken care to remove the excess electrolyte remaining on the surface of the membrane by wiping softly with a clean wiper, W_{dry} and V_{dry} are the weight and volume of dried the membrane. ρ_b is the density of 1-butanol.

The air permeability was measured by Air Permeability Tester (KES-F8-AP1, Kato Tech Co., Ltd., Japan) according to JISL1096, in order to investigate the effect of physically bonded structures on PVDF-HFP/PEG/PEGDMA nanofiber membrane.

The electrolyte uptake was obtained as follows: the membrane (2 cm×2 cm) was soaked in the liquid electrolyte, 1M lithium percholorate ($LiClO_4$) in ethylene carbonate (EC)/Diethyl carbonate (DEC) (1:1, v/v) (Tomiyama Purity Chemical Industries, Ltd., Japan), and then taken care to remove the excess electrolyte remaining on the surface of the membrane by wiping softly with a clean wiper. The electrolyte uptake was then calculated using equation (2) [15]:

$$\text{Electrolyte uptake (\%)} = \frac{M_f - M_i}{M_i} \times 100 \quad (2)$$

where M_i and M_f are the mass of the PVDF-HFP/PEG/PEGDMA nanofiber membrane before and after soaking, respectively.

5.2.3 Electrochemical measurements

The ionic conductivity (σ) was determined by VSP the multichannel potentiostat (Bio Logic SAS, France). The coin cell (CR2032 type) was assembled in a glove box filled with Ar gas. The membrane was soaked in a 1 M $LiClO_4$ in EC/DEC (1:1, v/v) and sandwiched between two parallel stainless-steel (SS) plates as current collectors, and then packed. The frequency ranged from 1 MHz to 10 kHz. The ionic conductivity was calculated from the bulk resistance (R) according to equation (3) [16]:

$$\sigma = \frac{l}{RS} \quad (3)$$

where l is the thickness of the membrane, S is the contact area between the membrane and SS plates (φ= 1.55 cm). The bulk resistance was obtained from the complex impedance diagram.

For measurement of cell cycling performance of the membrane, the coin cell was assembled in a glove box. The cells were soaked in a 1 M $LiClO_4$ in EC/DEC (1:1,

v/v), and the membrane was sandwiched between anode and cathode as current collectors, and packed. The cathode was lithium foil and anode was made up of MAG (Massive Artificial Graphite) on the Ni-mesh. The cycling performance of the membrane was evaluated by BTS2004W (NAGANO Co., Ltd, Japan) in the voltage range of 0.02-2.8 V. All electrochemical measurements were carried out at ambient temperature (T=23-25 °C).

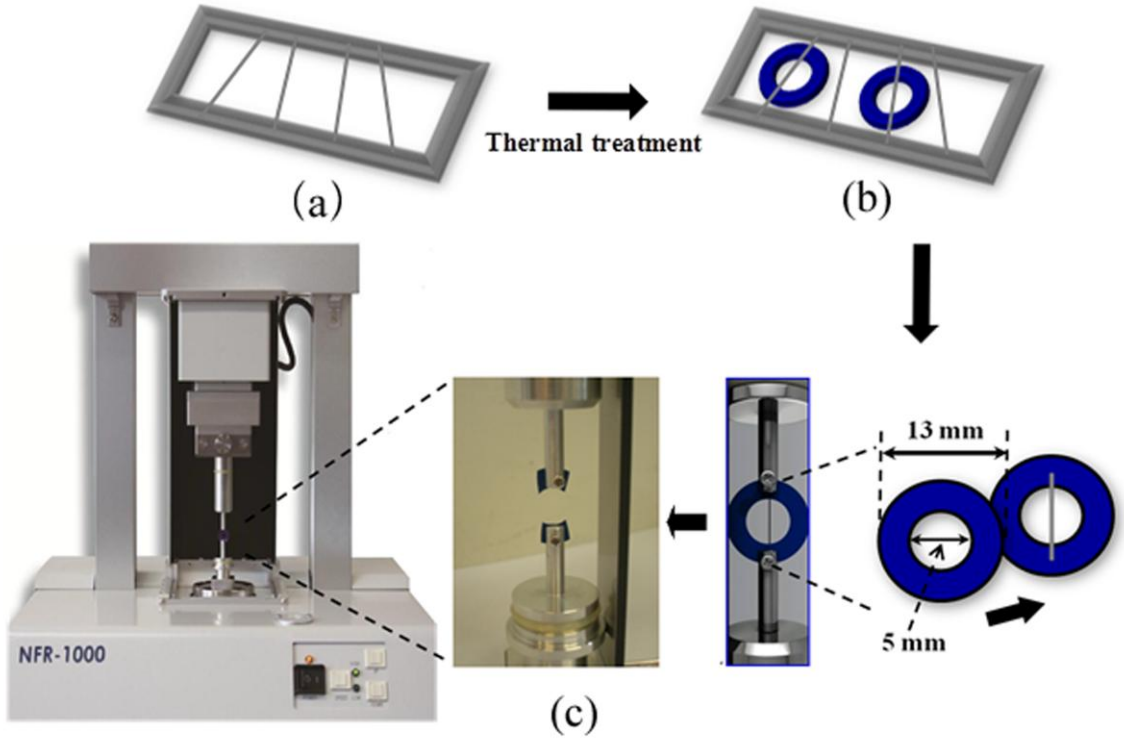

Figure 1 Schematic of sample preparation (a) metal sample frame, (b) paper cutting sheet for collecting single nanofibers, c) sample holder.

5.3 Results and discussion

5.3.1 Morphologies

In general, PVDF-HFP copolymer can be dissolved in the mix-solvent of acetone and *N, N*-dimethylformamide (DMF) [17], but the spinnability was not as stable as in the mix-solvent of acetone and DMAc, which was used in this study. Fig. 2 shows SEM images of thermal-treated electrospun PVDF-HFP/PEG/PEGDMA nanofiber membranes with composition ratio of 10/0/0, 6/4/0, 6/3/1, 6/2/2, 6/1/3, and 6/0/4. Inset in Fig. 2 presents SEM images of cross-section of each PVDF-HFP/PEG/PEGDMA nanofiber membrane. As can be seen from cross-section images in Fig. 2, all samples maintain fiber morphology after thermal-treatment. The pure PVDF-HFP nanofiber membrane was found to form uniform fibers with diameter around 310±40 nm (Fig. 2a). However, the morphologies of PVDF-HFP/PEG/PEGDMA nanofiber membranes were quite different from that of pure PVDF-HFP nanofibers. The fiber became thicker and inhomogeneous with increasing the amount of PEGDMA duing to the formation of physically bonded structures (Fig. 2b-f). The average fiber diameters of PVDF-HFP-640, PVDF-HFP-631, PVDF-HFP-622, PVDF-HFP-613, and PVDF-HFP-604 membranes were 419±160, 652±270, 660±205, 701±186, 738±461.5 nm, respectively. Among them, excellent bonded structures without large aggregation was formed in case of PVDF-HFP-613, as evidenced by cross-section SEM image (Fig. 2e) Zhao et al. reported that if the amount of PEGDMA was small, polymerization happened inside or on the surface of the electrospun nanofibers after thermal treatment. On the other hand, when a large amount of PEGDMA was added, the redundant PEGDMA oligomers tended to

leach out from the polymer and bonded between fibers. In this study, when the ratio of PVDF-HFP/PEG/PEGDMA was 6/0/4, very thick fibers appeared and a wider fiber diameter distribution was observed (Fig. 2f). It was considered that excess amounts of PEGDMA oligomers were added, as a result, they aggregated to cross-link between the fibers and made it like a film. This result also agreed well with Zhao and coworkers [17]. Fig. 2g and f present SEM images of thermal-treated PVDF-HFP-613 nanofibers before and after washing in ethanol and distilled water. The physically bonded structures clearly disappeared, and the fiber diameters decreased after washing (Fig. 2f). Hence, the physically bonded structures were considered to be fabricated by thermal treatment of PEGDMA on the surface of fibers.

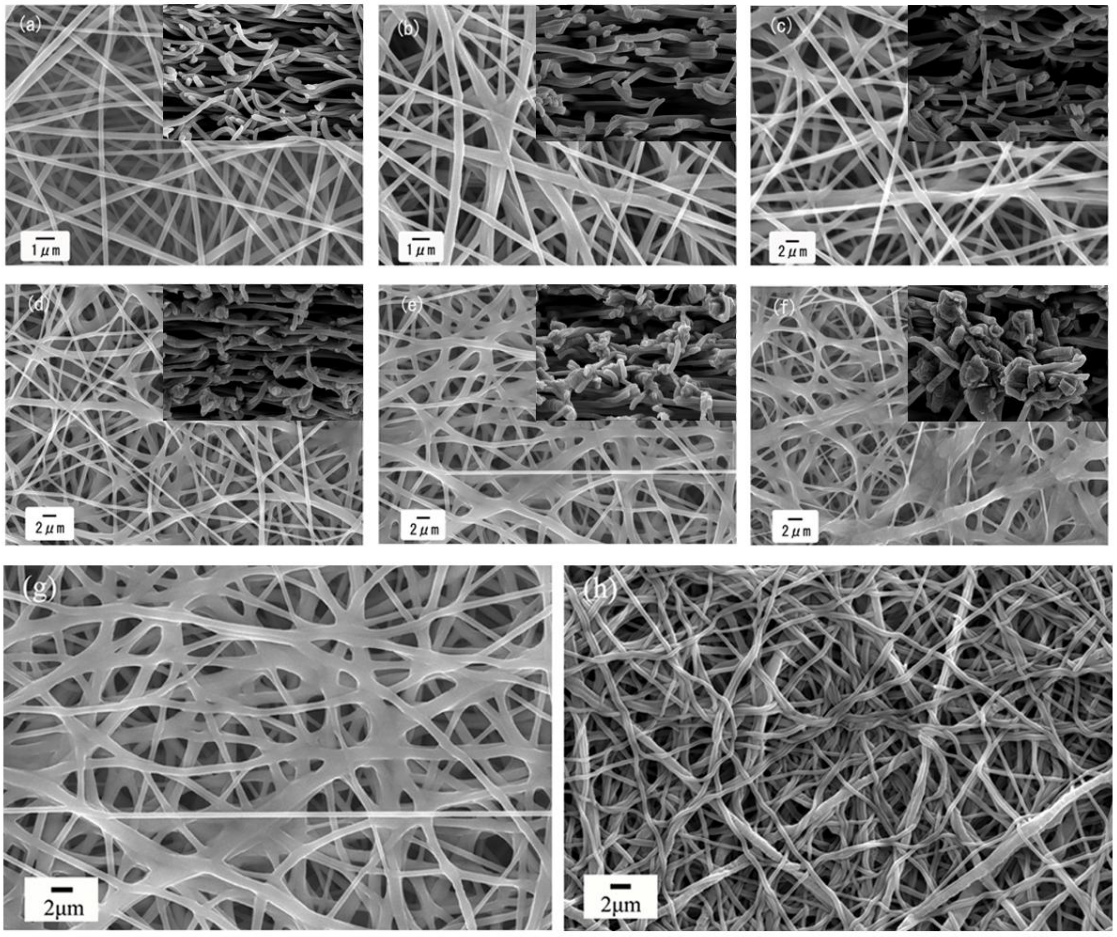

Figure 2 SEM images of electrospun PVDF-HFP/PEG/PEGDMA nanofibers with each composition ratio after thermal treatment (a) 10/0/0, (b) 6/4/0, (c) 6/3/1, (d) 6/2/2, (e) 6/1/3, (f) 6/0/4. And thermal-treated electrospun PVDF-HFP-613 nanofibers before (g) and after (h) wash in ethanol and distilled water

5.3.2 FT-IR analysis

FT-IR spectroscopy was used to investigate the changes in the chemical structures and molecular interactions of electrospun PVDF-HFP/PEG/PEGDMA nanofibers. Fig. 3(I) presents FT-IR spectra of PEGDMA oligomer (g) and electrospun PVDF-HFP/PEG/PEGDMA nanofibers with various composition ratios (Fig. 3I a-f) after thermal-treatment. As a result of thermal-treatment at 90 ^{o}C for 24 h, the C=C bond (1635 cm^{-1}), that was one of the characteristic peaks in pure PEGDMA, could not been observed in PVDF-HFP/PEG/PEGDMA nanofibers, and the C=O bond, which was another characteristic peak, was shifted from 1617 cm^{-1} to 1630 cm^{-1} with increasing the amount of PEGDMA [17]. The changes of these two peaks can be ascribed to the formation of PEGDMA cross-linked network, which is also described as interpenetrating polymer network (IPN) [18].

A mechanism was proposed to explain the fabrication of IPN-like structure (Fig. 3II). The PVDF-HFP copolymers were randomly mixed with PEGDMA oligomer (as a network-forming agent) and PEG (as a plasticizer) in solution. Composite nanofibers were prepared by electrospinning. Then, the obtained nanofibers were thermal-treated and then PEGDMA oligomers tended to cross-link inside and on the surface of single fibers. Meanwhile, the added PEGDMA oligomers could also entangle in PVDF-HFP polymer chains and finally formed the IPN-like structures.

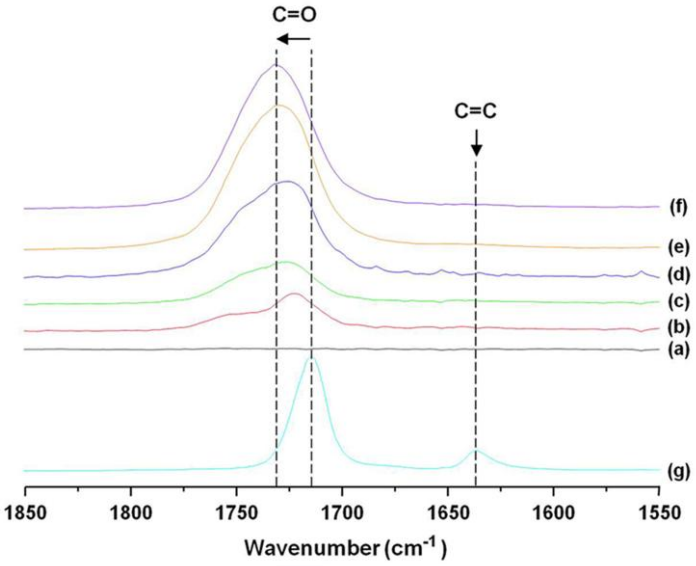

(I)

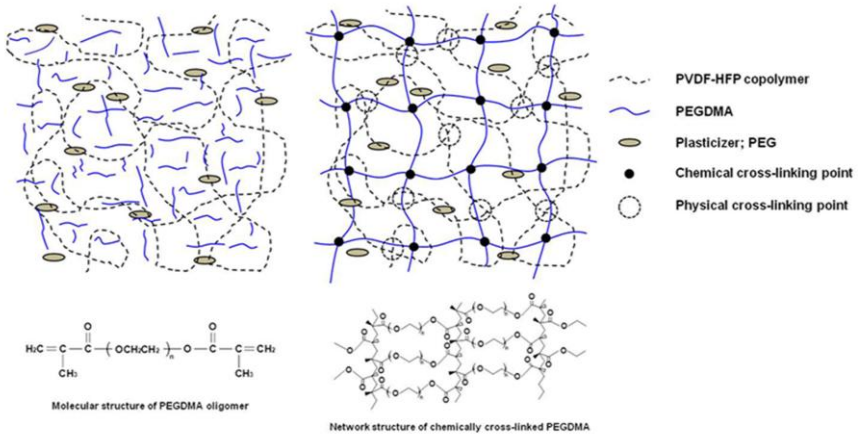

(II)

Figure 3 (I) FT-IR spectra of PEGDMA oligomer and electrospun PVDF-HFP/PEG/PEGDMA nanofibers with each composition ratio after thermal-treatment; (a) 10/0/0, (b) 6/4/0, (c) 6/3/1, (d) 6/2/2, (e) 6/1/3, (f) 6/0/4, (g) pure PEGDMA oligomer. And (II) schematic illustration of PEGDMA chemically cross-linked structure in PVDF-HFP/PEG/PEGDMA nanofiber (IPN-like networks).

5.3.3 Mechanical properties

Fig. 4 presents the stress-strain curves of electrospun PVDF-HFP/PEG/PEGDMA nanofiber membranes (I) and single nanofibers (II) with various composition ratios. The PVDF-HFP-613 nanofiber membrane (e in Fig. 4I) exhibited 1.9 times higher tensile strength and 2.8 times higher Young's modulus than pure PVDF-HFP nanofiber membrane (a in Fig. 4I). Moreover, the PVDF-HFP-604 (f in Fig. 4I) showed about 5 times higher Young's modulus than pure PVDF-HFP nanofiber membrane (a in Fig. 4I), while elongation at break was decreased to 47.4%, suggesting that the elasticity of these nanofiber membranes are reinforced by the formation of chemically cross-linked networks (IPN-like structures) and physically bonded structures on the fiber surface after thermal-treatment. Lalia et al. [19] reported that improved mechanical properties of PVDF-HFP nanofiber membrane by including nanocrystalline cellulose (NCC). Enhanced mechanical properties of PVDF-HFP nanofiber membrane were 6.1 MPa and 8.1 MPa corresponding to Young's modulus and tensile strength, respectively. Compared to the above material, PVDF-HFP-613 nanofiber membrane has even better mechanical properties, which are 28.1 MPa and 19.0 MPa corresponding to Young's modulus and tensile strength, respectively. Furthermore, in order to estimate intrinsic mechanical properties of a single nanofiber, tensile tests of electrospun PVDF-HFP/PEG/PEGDMA single nanofibers with various composition ratios were carried out. The elongation at break decreased greatly as increasing PEGDMA content because the motion of molecule chain in PVDF-HFP was prevented by cross-linked networks (IPN-like structure) of PEGDMA [17], whereas Young's modulus was improved around 4 times from 0.81 GPa to 3.39 GPa (a, e in Fig. 4II) attributed to the

chemically cross-linked networks of PEGDMA formed in the PVDF-HFP/PEG/PEGDMA single nanofiber.

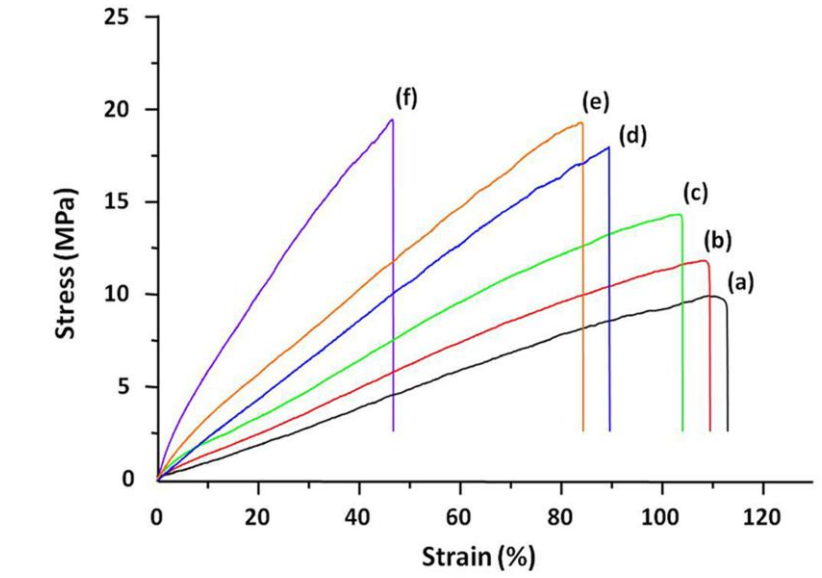

(I)

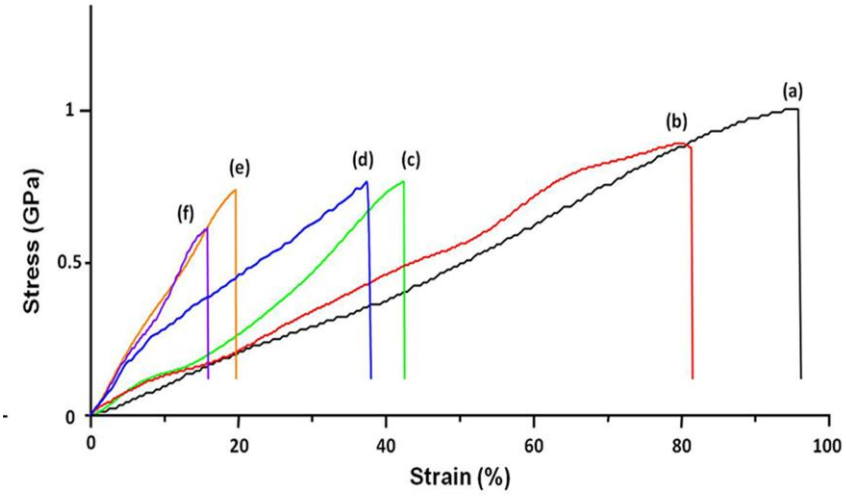

(II)

Figure 4 Stress-Strain (S-S) curves of electrospun PVDF-HFP/PEG/PEGDMA nanofiber membranes (I) and single nanofiber (II) with each composition ratio after thermal treatment; (a) 10/0/0, (b) 6/4/0, (c) 6/3/1, (d) 6/2/2, (e) 6/1/3, and (f) 6/0/4.

5.3.4 WAXD analysis

Fig. 5 presents WAXD patterns of electrospun pure PVDF-HFP nanofiber membrane (a), PVDF-HFP-613 nanofiber membranes before (b) and after (c) thermal-treatments, respectively. The two characteristic reflections at $2\theta = 18.2^{o}$ and 20.2^{o} correspond to the (100) and (020) crystalline peaks of α-phase in PVDF-HFP [20]. The characteristic peaks of both PVDF-HFP and PEGDMA can be confirmed in Fig. 5b. However, after thermal-treatment, the peak at $2\theta = 20.2^{o}$ disappeared and a broad diffraction peak at $2\theta = 20.5^{o}$ was observed (Fig. 5c). This due to the interaction between the PEGDMA cross-linked networks and the PVDF polymer chains [21]. Meanwhile, the relative intensity of peak at $2\theta = 19.7^{o}$ decreased and a small shoulder peak can be observed after thermal-treatment. It is considered that the crystalline of PEGDMA decreased because of the formation of cross-linked structure.

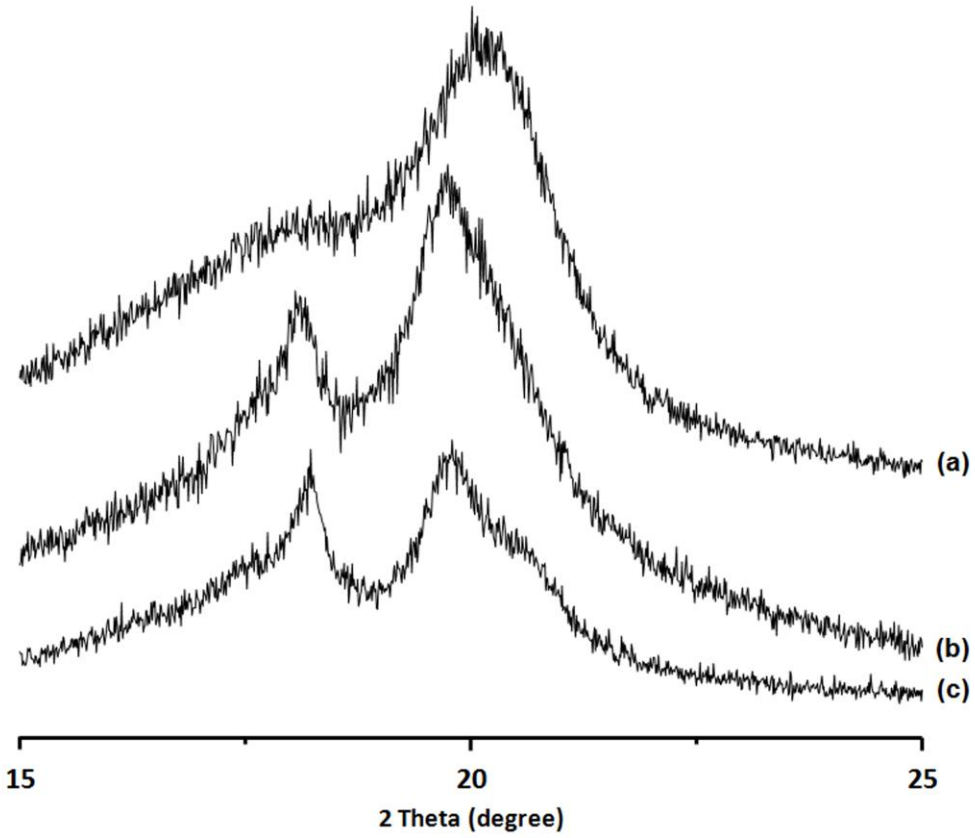

Figure 5 WAXD patterns of electrospun pure PVDF-HFP nanofiber membrane (a), PVDF-HFP-613 nanofiber membranes before (b) and after (c) thermal-treatments.

5.3.5 Cell cycling performance

The PVDF-HFP-613 nanofiber membrane, with good mechanical property, was used for cell cycling test and compared with the commercial separator (TF4850, NIPPON KODOSHI CO., Japan) used in lithium-ion batteries (LIBs). The characteristic data were summarized in Table 1. The electrolyte uptake of PVDF-HFP-613 nanofiber membrane was much higher than that of commercial TF4850 separator because of higher porosities. Electrolyte uptake of the separator is a very important factor as it is directly related to LIBs performance. As Saito and coworkers [22] proposed, the liquid electrolyte infiltrated into the pores of the nanofiber membrane from outside, trapped in the pores, and subsequently penetrated into the polymer chain to form a swollen gel.

The bulk resistance values (*R*) measured by AC impedance spectra were 0.94 Ω, 1.68 Ω, and 2.02 Ω, corresponding to thin and thick PVDF-HFP-613 nanofiber membranes and TF4850 separator, respectively. Thus, the ionic conductivity (σ) can be calculated according to Eq. (4). The calculated σ values were 1.70×10^{-3}, 1.42×10^{-3}, and 1.31×10^{-3} S/cm, corresponding to thin (29-31 μm), thick (44-46 μm) PVDF-HFP-613 nanofiber membranes and TF4850 separator, respectively. The electrospun PVDF-HFP-613 nanofiber membranes showed great ionic conductivity at ambient environment compared to commercial TF4850 separator. Moreover, higher ionic conductivity can be obtained as the membrane thickness decreases. Lithium ion migrates through the porous membrane via two different environments: the liquid state, which is within the porous structure, and the gel state, which is the swollen polymer matrix. Saito and coworkers emphasized that the ionic conductivity of the porous membrane is mainly determined by the ionic mobility inside the gel state. Therefore, higher electrolyte uptake

was considered to have dominant contributions to the improvement of the ionic conductivity.

Finally, cell cycling performance was shown in Fig. 6. The cell cycling performance of thin (29-31 μm) PVDF-HFP-613 nanofiber membrane was close to theoretical figure (372 mA/g) [23], probably due to uninterrupted ion diffusion. On the other hands, TF4850 and thick PVDF-HFP-613 nanofiber membrane showed lower discharge capacity. It is suggested the thickness and porosity of the separators make strong contributions to cell performance. However, in this study, the cell performance of nanofiber membrane with the thickness of 20-25 μm was not able to measure in half-cell, because the dendrites grow bigger and faster in half-cell than in the full-cell. The full-cell performance of thinner nanofiber membranes are needed to be investigated in subsequent work.

Table 1 The characteristic data of comparative measured samples.

Sample	Thickness (μm)	Porosity (%)	Air permeability ($cc/cm^2/sec$)	Electrolyte uptake (%)	Bulk resistance (Ω)
TF4850 (cellulose)	**50**	**65**	**1.31**	**136**	**2.02**
PVDF-HFP-613	**29-31**	**71**	**1.56**	**212**	**0.94**
PVDF-HFP-613	**44-46**	**69**	**0.98**	**205**	**1.68**

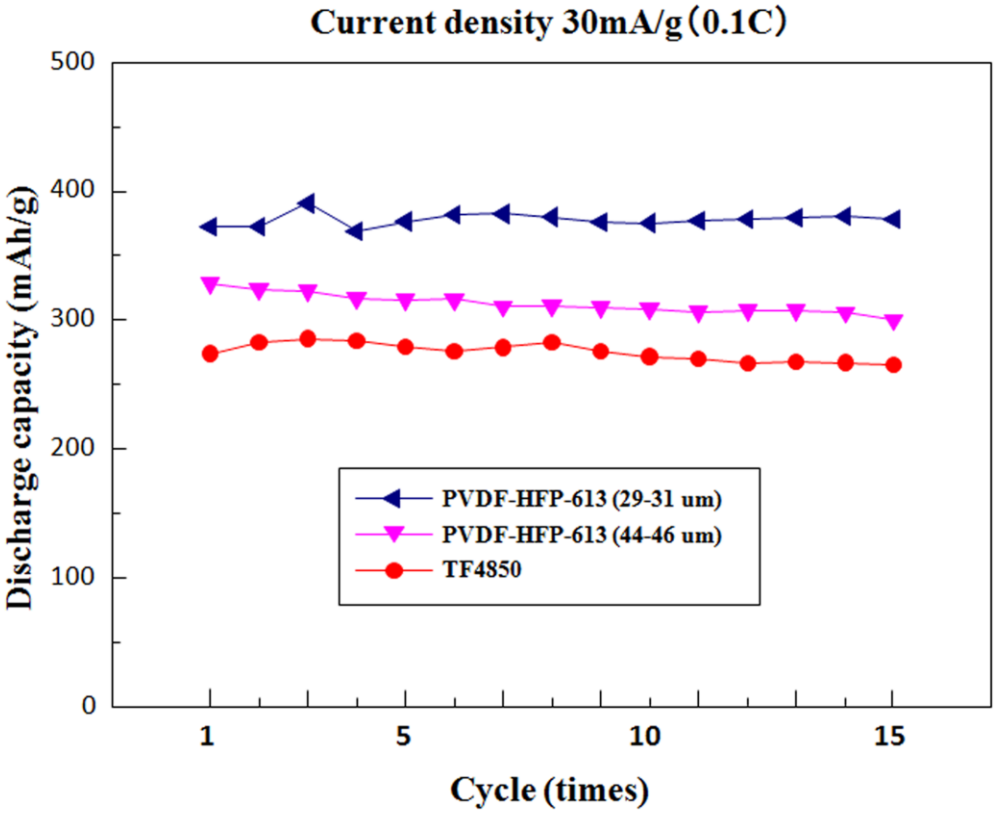

Figure 6 Characteristic of cycling performance

5.4 References

[1] N. Reddy, H. Xu, Y. Yang, Unique Natural-Protein Hollow-Nanofiber Membrane Produced by Weaver Ants for Medical Applications, Biotechol. Bioeng. 108(7) (2011) 1726-1733.

[2] X. Chen, S. Wei, A. Yadav, R. Patil, J. Zhu, R. Ximenes, L. Sun, Z. Guo, Poly(propylene)/Carbon Nanofiber Nanocomposites: Ex Situ Solvent-Assisted Preparation and Analysis of Electrical and Electronic Properties, Macromol. Mater. Eng. 296(5) (2011) 434-443.

[3] R.M. Robert, M.G. Betar, V.T. Carl, S.H. Yang, All-carbon-nanofiber electrodes for high-energy rechargeable Li-O_2 batteries, Energy Environ. Sci. 4(8) (2011) 2952-2958.

[4] S.S. Choi, Y.S. Lee, C.W. Joo, S.G. Lee, J.K. Park, K.S. Han, Electrospun PVDF nanofiber web as polymer electrolyte or separator, Electrochim. Acta 50 (2-3) (2004) 339-343.

[5] Y.J. Kim, C.H. Ahn, M.B. Lee, M.S. Choi, Characteristics of electrospun PVDF/SiO_2 composite nanofiber membranes as polymer electrolyte, Mater. Chem. phys. 127(1-2) (2011) 137-142.

[6] C.L. Cheng, C.C. Wan, Y.Y. Wang, M.S. Wu, Thermal shutdown behavior of PVdF-HFP based polymer electrolytes comprising heat sensitive cross-linkable oligomers, J. Power Sources 144(1) (2005) 238-243.

[7] C.L. Cheng, C.C. Wan, Y.Y. Wang, Preparation of porous, chemically cross-linked, PVdF-based gel polymer electrolytes for rechargeable lithium batteries. J. Power Sources 134(2) (2004) 202-210.

[8] Q. Xiao, Z. Li, D. Gao, H. Zhang, A novel sandwiched membrane as polymer electrolyte for application in lithium-ion battery. J. Membr. Sci. 326(2) (2009) 260-264.

[9] Y. Ding, P. Zhang, Z. Long, Y. Jiang, F. Xu, W. Di, The ionic conductivity and mechanical property of electrospun P(VdF-HFP)/PMMA membranes for lithium ion batteries. J. Membr. Sci. 329(1-2) (2009) 56-59.

[10] K. Hwang, B. Kwon, H. Byun, Preparation of PVdF nanofiber membranes by electrospinning and their use as secondary battery separators. J. Membr. Sci. 378(1-2) (2011) 111-116.

[11] A.I. Gopalan, P. Santhosh, K.M. Manesh, J.H. Nho, S.H. Kim, C.G. Hwang, K.P. Lee, Development of electrospun PVdF－PAN membrane-based polymer electrolytes for lithium batteries. J. Membr. Sci. 325(2) (2008) 683-690.

[12] O. Ohsawa, K.H. Lee, B.S. Kim, S. Lee, I.C. Kim, Preparation and characterization of polyketone (PK) fibrous membrane via electrospinning. Polym. 51(9) (2010) 2007-2012.

[13] N. Kimura, H.K. Kim, B.S. Kim, K.H. Lee, I.S. Kim, Molecular Orientation and Crystalline Structure of Aligned Electrospun Nylon-6 Nanofibers: Effect of Gap Size. Macromol. Mater. Eng. 295(12) (2010) 1090-1096.

[14] B.S. Kim, I.S. Kim, Recent Nanofiber Technologies: A Perspective for a Special Issue of Polymer Reviews, Polym. Rev. 51(3) (2011) 235-238.

[15] A. Ren, Y. Liu, K. Sun, X. Zhou, N. Zhang, A microporous gel electrolyte based on poly(vinylidene fluoride-co-hexafluoropropylene)/fully cyanoethylated cellulose derivative blend for lithium-ion battery, Electrochim. Acta 54(6) (2009) 1888-1892.

[16] Y.H. Liao, X.P. Li, C.H. Fu, R. Xu, L. Zhou, C.L. Tana, S.J. Hu, W.S. Li, Polypropylene-supported and nano-Al_2O_3 doped poly(ethylene oxide)-poly(vinylidene fluoride-hexafluoropropylene)-based gel electrolyte for lithium ion batteries. J. Power Sources 196(4) (2011) 2115-2121.

[17] L/ Zhao, H. Zhang, X. Li, J. Zhao, C. Zhao, X. Yuan, Modification of Electrospun Poly(vinylidene fluoride-cohexafluoropropylene) Membranes Through the Introduction of Poly(ethylene glycol) Dimethacrylate. J. Appl. Polym. Sci. 111 (2009) 3104-3112.

[18] M.K. Song, J.Y. Cho, B.W. Cho, H.W. Rhee, Characterization of UV-cured gel polymer electrolytes for rechargeable lithium batteries, J. Power Source 110(1) (2002) 209-215.

[19] B.S. Lalia, Y.A. Samad, R. Hashaikeh, Nanocrystalline-Cellulose-Reinforced Poly(vinylidenefluoride-co-hexafluoropropylene) Nanocomposite Films as a Separator for Lithium Ion Batteries, J. Appl. Polym. Sci. 126(S1) (2012) 442-448.

[20] A.M. Stephan, K.S. Nahm, T.P. Kumar, M.A. Kulandainathan, G. Ravi, J. Wilson, Nanofiller incorporated poly(vinylidene fluoride–hexafluoropropylene) (PVdF–HFP) composite electrolytes for lithium batteries, J. Power Source159(2) (2006) 1316-1321.

[21] W. Li, L. Xu, D. Luo, H. Wu, J. Tu, M. Yang, A composite microporous gel polymer electrolyte prepared by ultra-violet cross-linking, Eur. Polym. J. 43(2) (2007) 522-528.

[22] Y. Saito, H. Kataoka, E. Quartarone, P. Mustarelli, Carrier Migration Mechanism of Physically Cross-Linked Polymer Gel Electrolytes Based on PVDF

Membranes, J. Phys. Chem. B 106(29) (2002) 7200-7204

[23] Y. Tao, M.T. McDowell, I. Ryu, H. Wu, N. Liu, L. Hu, W.D. Nix, Y. Cui, Interconnected Silicon Holow Nanospheres for Lithium-Ion Battery Anodes with Long Cycle Life, Nano Lett. 11(7) (2011) 2949-2954.

Chapter 6

Conclusions

Chapter 6

Conclusions

In chapter 2, as evidenced by polarized FTIR spectroscopy, the relative intensities of several absorbance bands, including the N-H stretching, and the amide I, amide II, and amide III vibrations are found to be different in the two polarized FTIR spectra (parallel polarized and perpendicularly polarized). For macroscopically well-aligned nylon-6 nanofibers, as the gap size of the negatively charged metal plates was increased, the intensity of the amide II vibration band was observed to increase relatively in the parallel-polarized FTIR spectra, while the intensity of the amide I vibration band was observed to increase relatively in the perpendicular polarized FTIR spectra. The results demonstrate that the polymer chains were arranged along the nanofiber axis on the molecular level in the macroscopically well-aligned, electrospun nylon-6 nanofibers. Moreover, the molecular orientation of the polymer chains with the nanofibers was strongly affected by the gap size of the negatively charged metal plates used as the collector.

In chapter 3, the improved the mechanical strength of electrospun PMP fibrous membranes was successfully fabricated via inducing thermal-treatment and stretching process. The electrospun ultra-fine PMP fibers without beads were produced by mixture of solvents, cyclohexane/acetone/DMF; 80/5/15 (w/w/w). The crystallinity of electrospun PMP fibers were greatly increased by thermal-treatment and stretching process. It is confirmed by WAXD that the thermal-treatment occurred in changing from form-II to stable form-I of PMP fibers. Finally, the electrospun PMP fibrous membrane produced by

thermal-treatment at 180 ^{o}C and stretching process exhibited around 4.1 times higher tensile strength and 14.1 times higher Young's modulus than pure PMP fibrous membrane. In this future work, the study of focusing on change of crystalline form of electrospun PMP fibers due to it has five different crystalline forms.

In chapter 4, nylon-6 nanofiber mats with different contents of Fe^{2+} ions were successfully fabricated via electrospinning. SEM analysis showed unique morphological features, such as a spider's-web-like morphology, indicating the formation of very fine nanofibers with a diameter of 30 nm between the nylon-6 nanofibers in the nylon-6/$FeCl_2$ nanofiber mats. Moreover, such very fine nanofibers with diameters of about 30 nm considerably increased with increasing content of additive Fe^{2+} ions. FTIR, WAXD and DSC measurements suggested that the crystalline structures (e.g. the α- and γ-form crystals of nylon-6) and the crystallinity of the resulting electrospun nylon-6/$FeCl_2$ nanofibers were altered by the additives. The mechanical properties of the resulting electrospun nylon-6/$FeCl_2$ nanofibers were significantly dependent on the amount of additive Fe^{2+} ions.

In chapter 5, the reinforced electrospun composite nanofiber membranes are successfully fabricated via electrospinning and thermal-treatment. The presence of physically bonded structures and chemically cross-linked networks were confirmed by using SEM, FT-IR, and WAXD. The mechanical properties of both single nanofiber and nanofiber membrane were improved by chemically PEGDMA cross-linking and physically bonded structures. The prepared PVDF-HFP-6/1/3 nanofiber membrane has a higher porosity, electrolyte uptake, and bulk resistance value than existing separator. Furthermore, PVDF-HFP-6/1/3 nanofiber membrane showed satisfied discharge capacity close to theoretical value. The reinforced electrospun composite PVDF-HFP nanofiber

membrane was considered to be a promising candidate as a separator in lithium-ion batteries.

In this study, I reported that electrospun fiber and/or membrane with improved mechanical properties, such as tensile strength, elongation, and Young's modulus. There are many various methods for improving fibers, and I examined especially including additives, producing chemical cross-linked bonding structure, and inducing thermal-treatment with stretching process. The electrospun fiber and/or membrane were made it in all of three studies to improve the mechanical properties practically.

Chapter 7

Accomplishments

Chapter 7

7.1 Journal of publications

[1] **Naotaka Kimura**, Han-Ki Kim, Byoung-Suhk Kim, Keun-Hyung Lee, and Ick-Soo Kim, "Molecular Orientation and Crystalline Structure of Aligned Electrospun Nylon-6 Nanofibers; Effect of Gap Size." Macromol. Mater. Eng. 295, (2010) 1090-6.

This paper is been adopted for cover.

[2] **Naotaka Kimura**, Byoung-Suhk Kim, Ick-Soo Kim, "Effects of Fe^{2+} ions on morphologies, microstructures and mechanical properties of electrospun nylon-6 nanofibers" Polym. Int. Early View (Online Version of Record published before inclusion in an issue).

[3] **Naotaka Kimura**, Takeaki Sakumoto, Yuki Mori, Kal Wei, Byoung-Suhk Kim, Kyung-Hun Song, Ick-Soo Kim, "Fabrication and characterization of reinforced electrospun poly (vinylidene fluoride-cohexafluoropropylene) nanofiber membranes" Compos. Sci. Technol. Accepted on Dec. 2013.

[3] Byoung-Suhk Kim, **Naotaka Kimura**, Han-Ki Kim, Kei Watanabe, Ick Soo Kim, "Thermal insulation, antibacterial and mold properties of breathable nanofiber-laminated wallpapers." J. Nanosci. Nanotechnol. 11, (2011) 4929-33.

[4] Kai Wei, Jian-Hua Xia, **Naotaka Kimura**, Taiki Nakamura, Byoung-Suhk Kim, Ick-Soo Kim, "Tensile Strength of Single Electrospun Nanofibers." Adv. Mater. Res. 175, (2011) 294-8.

[5] **Naotaka Kimura**, Kei Watanabe, Taiki Nakamura, Byoung-Suhk Kim, Ick-Soo

Kim, “Nanofiber with Conductive Property.” SEN’I GAKKAISHI (Fiber and Industry) 672, (2011) 337-40.

7.2 Conferences

[1] **Naotaka Kimura**, Byoung-Suhk Kim, Ick-Soo Kim, “Preparation and Properties of Electrospun Nylon 6 Nanofibers Induced by the Effect of Additive Salt.” The Connect World Conference & Expo 2011, Boston, USA (2011).

[2] **Naotaka Kimura**, Han-Ki Kim, Byoung-Suhk Kim, Ick-Soo Kim, “Study on Molecular Orientation and Crystalline Structure of Aligned Electrospun Nylon 6 Nanofibers Affected Gap Size.” The 11th Asian Textile Conference, Daegu, Korea (2011).

[3] **Naotaka Kimura**, Byoung-Suhk Kim, Ick-Soo Kim, “The effect of Mechanical Properties of Electrospun Nylon 6 Composite Nanofibers by Crystalline Changes of Salt Additives.” 2nd Nano Today Conference, Hawaii, USA (2011).

[4] **Naotaka Kimura**, Byoung-Suhk Kim, Keun-Hyung Lee, Ick-Soo Kim, “Characterization and Fabrication of Aligned Nylon 6 Nanofibers.” The 60th Society of Polymer Science Conference, Osaka, JPN (2011).

[5] **Naotaka Kimura**, Byoung-Suhk Kim, Ick-Soo Kim, “The Effect of Nylon 6 nanofibers by Affected Plate Gap Size.” The 64th Textile Machinery Society of Japan Conference, Osaka, JPN (2011).

[6] **Naotaka Kimura**, Yuki Mori, Kai Wei, and Ick-Soo Kim, “Fabrication of Sheet with Ultrafine Carbon Nanofibers via Electrospinning.” The 7th Asian

Conference on Electrochemical Power Sources, Osaka, JPN (2013).

[7] **Naotaka Kimura**, Takeaki Sakumoto, Yuki Mori, Kal Wei, Byoung-Suhk Kim, Kyung-Hun Song, Ick-Soo Kim, "Fabrication and characterization of reinforced electrospun poly (vinylidene fluoride-cohexafluoropropylene) nanofiber membranes" International Conference on Nanoscience and Nanotechnology, Adelaide, AUS (2014).

7.3 Symposiums

[1] Yuki Mori, **Naotaka Kimura**, Kai Wei, Yoong Ahm Kim, Ick Soo Kim, "Fabrication of Thin and Unique Carbon Nanofibers Based on the Polyacrylonitrile/Poly (methyl methacrylate) via Electrospinning." The 6th International Symposium on High-Tech Fiber Engineering for Young Researcher, Aug. 20-25, Seoul, Korea (2013) P. 75 (PS8).

7.4 Patents

[1] Ick-Soo Kim, Byoung-Suhk Kim, Kei Watanabe, **Naotaka Kimura**, Kyu-Oh Kim, Yaeko Akada, Akinori Inau, "Composite nanofiber with dispersion of composition nanofiber, MWCNT with POSS" Japanese patent application No. 2010-186705.

[2] Ick-Soo Kim, Byoung-Suhk Kim, Kei Watanabe, **Naotaka Kimura**, Hea-Rim

Kim, Jae-hwan Lee, “Method For Manufacturing Metal Nanostructure and Metal Nanostructure Manufactured by The Method” 12963764.

[3] Ick-Soo Kim, Byoung-Suhk Kim, Kei Watanabe, **Naotaka Kimura**, Yu-Jin Lee, Jae-hwan Lee, “Fabrication Device of Separator” Japanese patent application No.2011-025512.

[4] Ick-Soo Kim, Byoung-Suhk Kim, Kei Watanabe, **Naotaka Kimura**, Kyu-Oh Kim, Jae-hwan Lee, “Separator, Fabrication Way of Separator, and Fabrication Device of Separator” Japanese patent application No. 2011-61736.

[5] Ick-Soo Kim, Byoung-Suhk Kim, Kei Watanabe, **Naotaka Kimura**, Hae-Rim Kim, Jae-hwan Lee, “Fabrication Device of Separator” Japanese patent application No.2011-61837.

[6] Ick-Soo Kim, Byoung-Suhk Kim, Kei Watanabe, **Naotaka Kimura**, Kyu-Oh Kim, Jae-hwan Lee, “Fabrication way and Device of Polyolefin nanofiber membrane, and Separator” Japanese patent application No. 2011-61838.

[7] Ick-Soo Kim, Byoung-Suhk Kim, Kei Watanabe, **Naotaka Kimura**, Yu-Jin Lee, Jae-hwan Lee, “Fabrication Device of Separator” Japanese patent application No. 2011-61840.

[8] Ick-Soo Kim, Byoung-Suhk Kim, Kei Watanabe, **Naotaka Kimura**, Kyu-Oh Kim, Jae-hwan Lee, “Separator and Fabrication way of Separator” Japanese patent application No. 2011-61841.

[9] Ick-Soo Kim, Byoung-Suhk Kim, **Naotaka Kimura**, Taiki Nakamura, Jae-hwan Lee, “Fabrication Way of Composite Nanofiber, Composite Nanofiber, and Separator” Japanese patent application No. 2011-083213.

[10] Ick-Soo Kim, Byoung-Suhk Kim, Kei Watanabe, **Naotaka Kimura**, Hae-Rim

Kim, Jae-hwan Lee, “Separator, Fabrication Device and Way of Separator” Japanese patent application No. 2011-083214.

[11] Ick-Soo Kim, Byoung-Suhk Kim, Kei Watanabe, **Naotaka Kimura**, Hae-Rim Kim, Jae-hwan Lee, “Separator, Fabrication Device and Way of Separator” Japanese patent application No. 2011-165884.

[12] Ick-Soo Kim, Byoung-Suhk Kim, Kei Watanabe, **Naotaka Kimura**, Hae-Rim Kim, Jae-hwan Lee, “Separator, Fabrication Device and Way of Separator” Japanese patent application No. 2011-165885.

[13] Ick-Soo Kim, Byoung-Suhk Kim, Kei Watanabe, **Naotaka Kimura**, Hae-Rim Kim, Jae-hwan Lee, “Separator, Fabrication Device and Way of Separator” Japanese patent application No. 2011-172252.

[14] Ick-Soo Kim, Byoung-Suhk Kim, Kei Watanabe, **Naotaka Kimura**, Hae-Rim Kim, Jae-hwan Lee, “Separator, Fabrication Device and Way of Separator” Japanese patent application No. 2011-172259.

Chapter 8

Acknowledgments

Chapter 8

Acknowledgments

I would like to express my appreciation to my advisor Prof. Ick-Soo Kim of Faculty of Textile Science and Technology, Shinshu University for his invaluable advices and encouragement through the present investigations and opening my mind to excellent material, nanofiber. I also want to thank him for trusting my abilities to work on an application project of the nanofibers as interesting as it turned out to be and those elevated both my research and thinking/processing skills. I would also like to thank Prof. Y. Murakami, Prof. H. Fukunaga, Prof. Y. Hirata, and Prof. Lee for their supports of my graduate works in Shinshu University. And I acknowledge the support of Grant-in-Aid for the Global COE Program from the Ministry of Education, Culture, Sports, Science and Technology, Government of Japan. I also greatly thank to the time that I spent in Shinshu University during my graduate period, which allowed me to have invaluable opportunities to know good people and to build invaluable friendships with them. I am sincerely grateful to all of my friends for keeping my spirit up during the hard time and for having good time with me. I am very grateful to all the people at the Prof. Ick-Soo Kim's Research Lab, Faculty of Textile Science and Technology, Shinshu University who have given me much supports and helps so that I could successfully fulfill this work. Specifically, I appreciate and thank to Dr. Byoung-Suhk Kim and Dr. Kai Wei for their many assistances, helps, and continuous encouragements. They gave me their strong interests, their novel ideas, interesting aspects, and helpful suggestions during this work.